Article

Current Biology

The focal adhesion protein β-parvin controls cardiomyocyte shape and sarcomere assembly in response to mechanical load

Highlights

- β-parvin makes membrane protrusion and serial sarcomere assembly in cardiomyocytes
- Physiological loads induce cardiomyocyte elongation via β-parvin/PIX/Rac1-signaling
- β-parvin plays a key role in exercise-induced cardiac hypertrophy in mice

Authors

Ingo Thievessen, Frank Suhr, Silvia Vergarajauregui, ..., Ben Fabry, Wilhelm Bloch, Reinhard Fässler

Correspondence

ingo.thievessen@fau.de (I.T.), faessler@biochem.mpg.de (R.F.)

In brief

Thievessen et al. identify β-parvin as novel mechanosensor in cardiomyocytes. β-parvin activates PIX/Rac1 to induce membrane protrusion, serial sarcomere assembly, and cardiomyocyte elongation in response to physiological mechanical load. Loss-of-function studies in mice reveal that β-parvin orchestrates exercise-induced cardiac hypertrophy *in vivo*.

Thievessen et al., 2022, Current Biology *32*, 1–15
July 25, 2022
https://doi.org/10.1016/j.cub.2022.05.047

CellPress

Current Biology

CellPress

Article

The focal adhesion protein β-parvin controls cardiomyocyte shape and sarcomere assembly in response to mechanical load

Ingo Thievessen,[1,2,3,*] Frank Suhr,[4,5] Silvia Vergarajauregui,[3,6] Ralph T. Böttcher,[1] Klara Brixius,[4] Georg Rosenberger,[7] Oliver Dewald,[8] Bernd K. Fleischmann,[9] Alexander Ghanem,[10] Marcus Krüger,[11] Felix B. Engel,[3,6] Ben Fabry,[2,3] Wilhelm Bloch,[4] and Reinhard Fässler[1,12,*]

[1]Max-Planck-Institute of Biochemistry, Department of Molecular Medicine, Martinsried, Germany
[2]Biophysics Group, Department of Physics, Friedrich-Alexander-Universität Erlangen-Nürnberg, Erlangen, Germany
[3]Muscle Research Center Erlangen (MURCE), Friedrich-Alexander-University of Erlangen-Nuremberg, Erlangen, Germany
[4]Department of Molecular and Cellular Sport Medicine, German Sport University Cologne, Cologne, Germany
[5]Exercise Physiology Research Group, Biomedical Sciences Group, KU Leuven, Leuven, Belgium
[6]Experimental Renal and Cardiovascular Research, Department of Nephropathology, Institute of Pathology, Friedrich-Alexander-Universität Erlangen-Nürnberg, Erlangen, Germany
[7]Institute of Human Genetics, University Medical Center Hamburg-Eppendorf, Hamburg, Germany
[8]Department of Cardiac Surgery, Medical Campus University of Oldenburg, Oldenburg, Germany
[9]Institute of Physiology I, Life and Brain Center, Medical Faculty, University of Bonn, Bonn, Germany
[10]Department of Cardiology, Asklepios Klinik St. Georg, Hamburg, Germany
[11]Institute for Genetics and Cologne Excellence Cluster on Cellular Stress Responses in Aging-Associated Diseases (CECAD), University of Cologne, Cologne 50931, Germany
[12]Lead contact
*Correspondence: ingo.thievessen@fau.de (I.T.), faessler@biochem.mpg.de (R.F.)
https://doi.org/10.1016/j.cub.2022.05.047

SUMMARY

Physiological and pathological cardiac stress induced by exercise and hypertension, respectively, increase the hemodynamic load for the heart and trigger specific hypertrophic signals in cardiomyocytes leading to adaptive or maladaptive cardiac hypertrophy responses involving a mechanosensitive remodeling of the contractile cytoskeleton. Integrins sense load and have been implicated in cardiac hypertrophy, but how they discriminate between the two types of cardiac stress and translate mechanical loads into specific cytoskeletal signaling pathways is not clear. Here, we report that the focal adhesion protein β-parvin is highly expressed in cardiomyocytes and facilitates the formation of cell protrusions, the serial assembly of newly synthesized sarcomeres, and the hypertrophic growth of neonatal rat ventricular cardiomyocytes (NRVCs) *in vitro*. In addition, physiological mechanical loading of NRVCs by either the application of cyclic, uni-axial stretch, or culture on physiologically stiff substrates promotes NRVC elongation in a β-parvin-dependent manner, which is achieved by binding of β-parvin to α/β-PIX, which in turn activates Rac1. Importantly, loss-of-function studies in mice also revealed that β-parvin is essential for the exercise-induced cardiac hypertrophy response *in vivo*. Our results identify β-parvin as a novel mechano-responsive signaling hub in hypertrophic cardiomyocytes that drives cell elongation in response to physiological mechanical loads.

INTRODUCTION

Cardiomyocytes sense and respond to an increase in mechanical load by activating specific signaling pathways that lead to distinct cardiac hypertrophies. Physiological cardiac hypertrophy occurs after repeated and healthy exercise and is characterized by a reversible, adaptive increase in heart muscle mass, which allows to process the elevated blood return (cardiac volume overload). Cardiac muscle mass increase is caused by the assembly of newly synthesized sarcomeres, which occurs in series and parallel to the existing ones, resulting in a finely balanced increase in cardiomyocyte length and width and eventually cardiac growth with preserved geometry of the heart ventricles.[1,2] Pathological cardiac hypertrophy, by contrast, develops in response to high blood pressure or aortic stenosis (cardiac pressure overload). Initially, the left ventricular muscle counterbalances the increased wall stress with an adaptive and reversible thickening of the ventricular wall. However, when wall stress continues, the ventricular muscle wall undergoes a maladaptive, progressive, and usually irreversible thickening, which results from the assembly of new sarcomeres almost exclusively in parallel to the existing ones leading to an over-proportional increase in cardiomyocyte width.[1–5] The consequences of the ventricular wall thickening can lead to secondary implications including increased stiffening of the ventricular wall and/or insufficient blood supply through coronary arteries resulting in cardiomyocyte death, formation of

Please cite this article in press as: Thievessen et al., The focal adhesion protein β-parvin controls cardiomyocyte shape and sarcomere assembly in response to mechanical load, Current Biology (2022), https://doi.org/10.1016/j.cub.2022.05.047

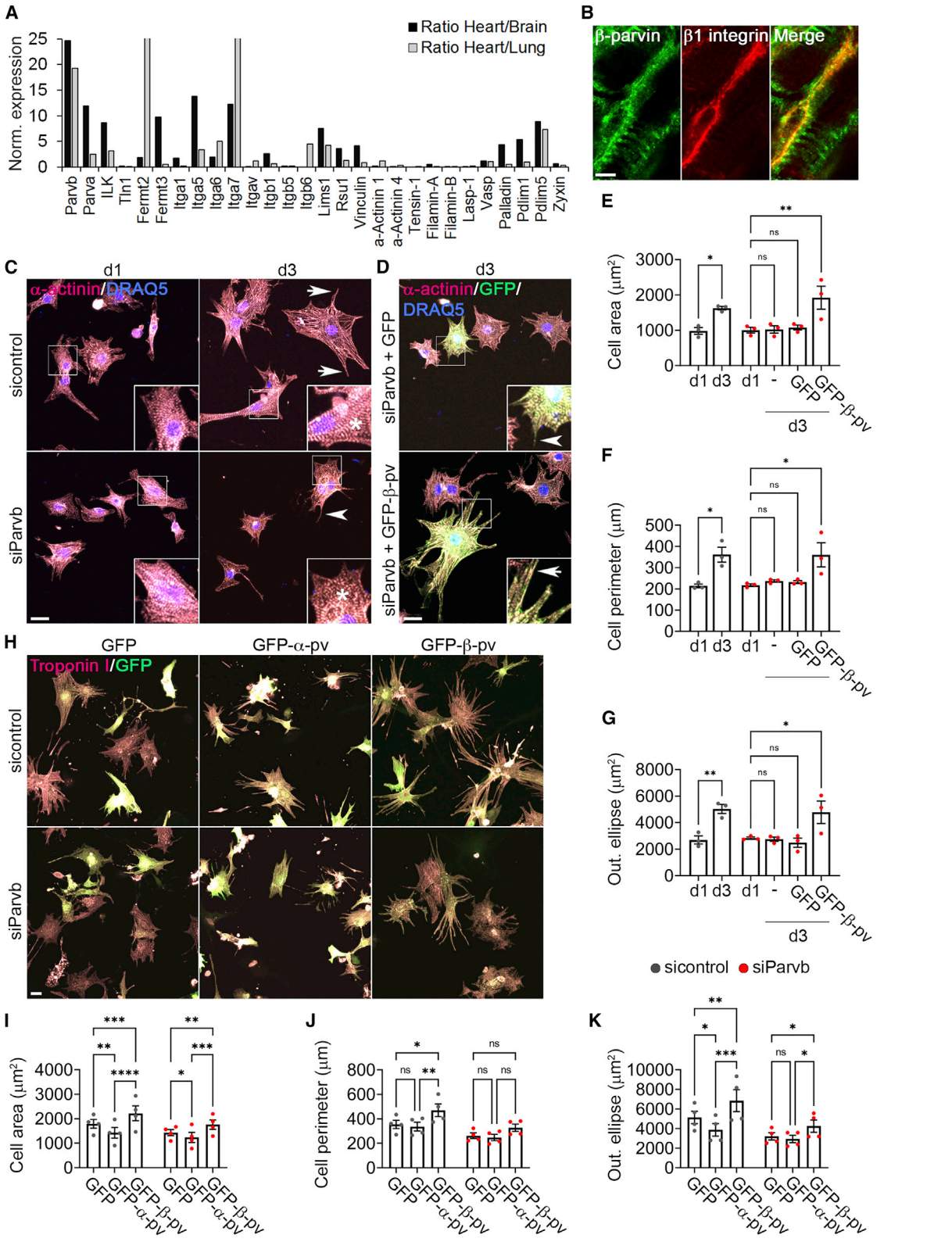

Figure 1. β-parvin abundance in cardiac tissue and role for NRVC hypertrophy and sarcomere-containing protrusions

(A) Expression levels of integrin-associated proteins in adult murine cardiac tissue relative to their expression levels in adult murine brain and lung determined by MS. Ratios of expression levels are normalized to ratios of proteasome subunit alpha type 1 (PSMA1) expression levels.

(legend continued on next page)

Please cite this article in press as: Thievessen et al., The focal adhesion protein β-parvin controls cardiomyocyte shape and sarcomere assembly in response to mechanical load, Current Biology (2022), https://doi.org/10.1016/j.cub.2022.05.047

fibrotic tissue, and, in the end, cardiac insufficiency. Although a number of signaling pathways regulating actin dynamics, expression of distinct genes, and proteins have been associated with physiological[6–10] and/or pathological cardiac hypertrophy,[11–20] it is still an open question how cardiomyocytes differentiate between different mechanical loads, induce distinct signaling, and integrate newly synthesized contractile proteins into existing myofibrils.

Cardiomyocytes form characteristic protein assemblies around integrins at the sarcolemma called costameres. They connect Z-disks via integrins to the extracellular matrix (ECM), sense mechanical properties of the ECM and the actomyosin contractility,[21–23] and translate the mechanical information into biochemical signals with the help of mechanosensitive adaptor proteins and kinases. Although costameric proteins such as kindlin-2, vinculin, talin-1 and -2, α-parvin, or focal adhesion kinase (FAK) are required to preserve cardiac homeostasis and/or pressure-overload-induced cardiac hypertrophy,[24–31] it remains unclear whether distinct integrin-associated proteins exist that specifically respond to volume-overload and induce cardiac hypertrophy.

An essential ternary protein complex that associates with integrins in costameres and focal adhesions (FAs) of non-muscle cells consists of integrin-linked pseudo-kinase (ILK), LIM-only domain containing protein PINCH, and F-actin binding protein parvin (called IPP complex).[32–34] Mammals have a single *ILK* gene and protein, two *PINCH* genes encoding two isoforms (PINCH-1 and PINCH-2) and three *parvin* genes encoding three parvin isoforms (α-parvin, β-parvin, and γ-parvin).[35] The stabilization and recruitment of ILK, PINCH, and parvin proteins to integrin adhesion sites require the post-translational assembly into the IPP complex in the cytoplasm.[36] Studies with cultured cell lines indicate that IPP complexes can reorganize the actomyosin cytoskeleton through their ability to directly bind F-actin and modulate the activity of the Rho-family of small GTPases.[37–39]

Genetic studies in mice and fish have highlighted the importance of the IPP complex for heart function. In mice, deletion of the *α-parvin* (*Parva*) gene profoundly impairs formation and/or maintenance of cardiac sarcomeres, leading to embryonic death at midgestation,[40] whereas the cardiac-restricted deletion of the *ILK* gene leads to fibrosis and lethal heart dilation.[41] In zebrafish, expression of a parvin-binding-deficient ILK or the disruption of the *β-parvin* (*Parvb*) gene results in lethal heart contraction defects.[42] Although these studies showed that IPP complexes exert cardioprotective functions by inducing PI-3K/PKB/Akt signaling,[41,42] it is not known whether and how IPP orchestrates sarcomere assembly and safeguards the shape of hypertrophic cardiomyocytes, e.g., via regulating small GTPases including RhoA, Rac1, and Cdc42. These GTPases play important roles for myofibrillogenesis in cultured cardiomyocytes[3,43–46] and regulate volume- and/or pressure-overload-induced cardiac hypertrophy *in vivo*.[19,47]

In the present study, we identified β-parvin as a major mechano-sensor of costameres in cardiomyocytes, where it activates Rac1 and induces serial sarcomere assembly and cell elongation in response to cyclic stretch and growth on substrates with physiological stiffness. Moreover, mice lacking β-parvin expression (*Parvb*$^{-/-}$) failed to induce cardiac hypertrophy in response to exercise highlighting the central role of β-parvin for physiological cardiac hypertrophy.

RESULTS

β-parvin is abundant in cardiac muscle

To identify new integrin-associated proteins enriched in heart tissue, we determined the proteome of adult mouse hearts by mass spectrometry (MS) and compared the relative abundance of known adhesion proteins with their abundance in non-myocardial tissues.[48,49] Although the abundance of most adhesion proteins was similar between different tissues, Itga7, PDZ, and LIM domain 5 (PDLIM5) and β-parvin were highly enriched in adult hearts when compared with lung or brain (Figure 1A; Table S1). Although mutations in the human *Itga7* gene lead to congenital myopathy[50,51] and silencing of PDLIM5 to cardiac hypertrophy,[52] the role of β-parvin for cardiac function is elusive.

In line with the MS data, *in situ* hybridization on parasagittal sections of 14.5-day-old mouse embryos (E14.5) and western blots of adult mouse tissues confirmed the high expression levels of β-parvin in embryonic and adult hearts (Figures S1A and S1B). *β-parvin* levels were also high in skeletal muscle, peripheral ganglia, and megakaryocytes in the embryonic liver (Figure S1A). α-parvin expression, which is essential for heart development,[40] was high in most fetal and adult organs except heart and skeletal muscle, central nervous system, thymus, and fetal liver (Figures S1A and S1B). Notably, β-parvin colocalized with β1 integrin in costameres in murine adult left ventricular myocardial tissue (Figure 1B).

(B) Confocal micrograph showing β-parvin and β1 integrin immunofluorescence on cryosections of murine adult left ventricular tissue. Scale bars, 5 μm.
(C) Confocal micrographs showing α-actinin immunofluorescence and DRAQ5-staining of control- and *Parvb*-siRNA-treated NRVCs. Note increased cell size, well-organized α-actinin striation (asterisks), and long α-actinin positive cell protrusions in control- (arrows) but not *Parvb*- (arrowhead) siRNA NRVCs. Scale bars, 20 μm.
(D) Confocal micrographs showing α-actinin immunofluorescence, DRAQ5-staining, and GFP-fluorescence of *Parvb*-siRNA NRVCs expressing GFP or GFP-β-parvin. Note increased cell size and long α-actinin positive cell protrusions in GFP-β-parvin- (arrow) but not GFP (arrowhead)-expressing NRVCs. Scale bars, 20 μm.
(E–G) Quantification of cell area (E), cell perimeter (F), and outer bounding ellipse area (G) of control- and *Parvb*-siRNA NRVCs, and *Parvb*-siRNA NMVCs expressing GFP or GFP-β-parvin.
Data for (E)–(G) are shown as mean ± SEM from n = 3 independent biological replicates with 17–113 cells per group/replicate. ns, $p > 0.05$; *$p < 0.05$, **$p < 0.01$.
(H) Confocal micrographs showing cardiac troponin I immunofluorescence and GFP-fluorescence of control-siRNA- and *Parvb*-siRNA-treated NRVCs expressing GFP, GFP-tagged α-parvin, or GFP-tagged β-parvin. Scale bars, 20 μm.
(I–K) Quantification of cell area (I), cell perimeter (J), and outer bounding ellipse area (K) of control-siRNA and *Parvb*-siRNA NRVCs expressing GFP, GFP-tagged α-parvin, or GFP-tagged β-parvin. Data are shown as mean ± SEM from n = 4 independent biological replicates with 32–158 cells per group/replicate. ns, $p > 0.05$; *$p < 0.05$, **$p < 0.01$, ***$p < 0.001$, ****$p < 0.0001$.
See also Table S1 and Figures S1 and S2.

Please cite this article in press as: Thievessen et al., The focal adhesion protein β-parvin controls cardiomyocyte shape and sarcomere assembly in response to mechanical load, Current Biology (2022), https://doi.org/10.1016/j.cub.2022.05.047

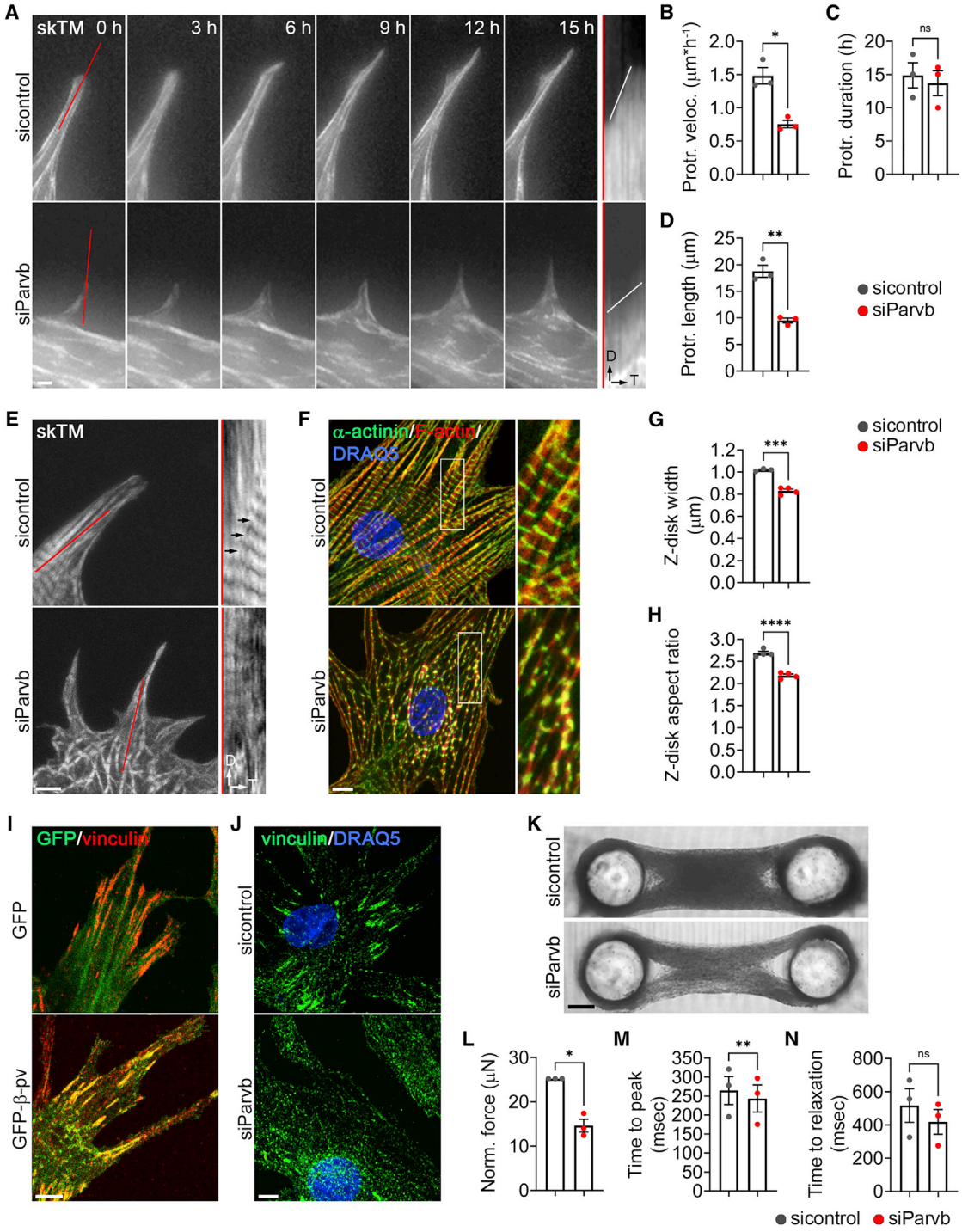

Figure 2. Role of β-parvin for NRVC morphology and contractility

(A) Epifluorescence time-lapse images of SCP growth in control- and *Parvb*-siRNA NRVCs; SCP marker skeletal muscle tropomyosin-GFP (skTM); 1 h frame rate. Red line shows line scan positioning parallel to the long axis of SCP for kymograph analyses (right) of SCP growth. D, distance; T, time. Scale bars, 5 μm.

(B–D) Quantification of protrusion velocity (B), duration (C), and distance (D) of control- and *Parvb*-siRNA NRVCs expressing skTM-GFP. Data are shown as mean ± SEM from n = 3 independent biological replicates with 5–49 protrusions per group/replicate. ns, $p > 0.05$; *$p < 0.05$, **$p < 0.01$, Student's t test.

(E) High-resolution confocal micrograph showing SCPs and cell body of live control- and *Parvb*-siRNA NRVCs expressing skTM-GFP as sarcomere marker; 1 h frame rate. Red line shows line scan positioning parallel to the long axis of SCP for kymograph analyses (right) of sarcomere assembly. Note serial assembly of new sarcomeres in front of existing ones in control- (arrows), but not *Parvb*-siRNA NRVCs. D, distance; T, time. Scale bars, 5 μm.

(F) High-resolution confocal micrographs showing α-actinin immunofluorescence, phalloidin-staining to visualize F-actin, and DRAQ5-staining in control- and *Parvb*-siRNA NRVCs. Note irregular α-actinin striation in *Parvb*- compared with control-siRNA NRVCs (inserts). Scale bars, 5 μm.

(legend continued on next page)

Please cite this article in press as: Thievessen et al., The focal adhesion protein β-parvin controls cardiomyocyte shape and sarcomere assembly in response to mechanical load, Current Biology (2022), https://doi.org/10.1016/j.cub.2022.05.047

β-parvin induces sarcomere-containing protrusions and the expansion of the cardiomyocyte surface area

To investigate β-parvin functions in cardiomyocytes, we depleted the mRNA with specific siRNAs in cultured neonatal (P3) rat ventricular cardiomyocytes (NRVCs) (Figure S2A) and measured several cell morphological parameters. Control-siRNA-treated NRVCs seeded on collagen for a period of 3 days showed well-organized striation of α-actinin (Figure 1C, asterisk) and an increase in cell area, perimeter, and longitudinal growth of cross-striated α-actinin-containing protrusions (sarcomere-containing protrusions, SCPs) measured with an outer bounding ellipse fitted around cells (Figures 1C, 1E–1G, and S2B–S2D). In contrast, *Parvb*-siRNA-treated NRVCs displayed a punctate organization of α-actinin (Figure 1C, asterisk) and did not increase cell area, perimeter, and outer bounding ellipse area (Figures 1C, 1E–1G, and S2D). Importantly, the defects were rescued upon lentiviral re-expression of siRNA-resistant GFP-β-parvin but not GFP (Figures 1D–1G), indicating that β-parvin promotes sarcomeric α-actinin organization, formation of SCPs, and expansion of the cardiomyocyte area.

Since α-parvin is also present in costameres and essential for normal and stressed cardiomyocytes,[31] we compared the effects of α- and β-parvin expression on cell morphology and SCPs of control- and *Parvb*-siRNA NRVCs. Although GFP-β-parvin overexpression in control-siRNA NRVCs increased cell area, perimeter, and outer bounding ellipse area (Figures 1H–1K), overexpression of GFP-α-parvin did not affect cell perimeter and decreased cell and outer bounding ellipse area (Figures 1H–1K). Similarly, expression of siRNA-resistant GFP-β-parvin rescued cell area and outer bounding ellipse area of *Parvb*-depleted NRVCs, whereas overexpression of GFP-α-parvin neither reversed the defects nor further impaired the cellular morphology (Figures 1H–1K). These data demonstrate that α-parvin cannot compensate β-parvin-induced SCP growth and expansion of the NRVC surface area.

β-parvin promotes leading edge protrusion, serial sarcomere assembly, and contractile force generation in NRVCs

To test whether β-parvin promotes the growth of SCPs and the assembly of sarcomeres in NRVCs, we developed long-term imaging to assess the morphodynamics of NRVCs. Epifluorescence live imaging of NRVCs expressing skeletal muscle tropomyosin-GFP (skTM-GFP) revealed that SCPs slowly and steadily grew over long-lasting time spans (15–20 h; Video S1). Kymograph analyses of SCP-dynamics in skTM-GFP expressing NRVCs revealed a significantly reduced protrusion velocity and length of SCPs in *Parvb*-siRNA NRVCs, whereas the protrusion duration remained unaffected (Figures 2A–2D; Video S1), demonstrating that β-parvin promotes the growth rate of SCPs.

To test whether β-parvin also influences the *de novo* formation of sarcomeres in growing SCPs, we performed high-resolution confocal imaging of live skTM-GFP expressing control- and *Parvb*-siRNA NRVCs (Video S2). Kymograph analyses of control-siRNA NRVCs revealed that several micrometers behind their leading edge new sarcomeres assembled in series in front of existing sarcomeres (Figure 2E, arrows; Video S2). Moreover, sarcomeres in growing SCPs displayed a retrograde motion toward the cell body (Figure 2E), reminiscent of the F-actin retrograde flow in the lamella of migrating fibroblasts. In sharp contrast, sarcomere assembly and retrograde flow were hardly detectable in the short SCPs of *Parvb*-siRNA NRVCs (Figure 2E; Video S2), indicating that β-parvin is also required for serial sarcomere assembly in growing SCPs. In addition, the sarcomere apparatus in the cell body of *Parvb*-siRNA NRVCs was disorganized with narrow, less elongated Z-disks (Figures 2F–2H) and showed a continuous, non-directional motion over time (Video S2), which was never observed in control-siRNA-treated NRVCs. Notably, GFP-tagged β-parvin localized to vinculin-positive adhesion sites (Figure 2I) and is required for normal adhesion site formation (Figure 2J) and substrate adhesion (Figures S3A and S3B) of NRVCs.

The sarcomere assembly and adhesion defects of *Parvb*-siRNA NRVCs suggest that β-parvin also affects cardiomyocyte contractility. To test this hypothesis, we generated three-dimensional (3D) cardiac microtissues in collagen gels by assisted self-assembly of NRVCs (Figure S3C). NRVCs in 3D microtissues displayed an elongated cell shape and an anisotropic α-actinin striation (Figure S3D). Spontaneous contractions extending across the entire 3D microtissue indicated that the NRVCs are mechanically and electrically coupled to each another (Video S3). Furthermore, treatment of 3D microtissues for 48 h with phenylephrine (PE), shown to promote cardiomyocyte force generation *in vivo* and *in vitro*,[53] significantly increased contractile forces of 3D microtissues (Figures S3E and S3F), which makes 3D microtissues suitable tissue surrogates for mechanistic analyses. In line with our hypothesis that cardiomyocytes require β-parvin for contractile force generation, 3D microtissues assembled by β-parvin-depleted NRVCs generated less contractile force than those made with the same number of control-siRNA-treated NRVCs (Figures 2K and 2L). Interestingly, the time between contraction onset and force peak as well as the force relaxation time were comparable between microtissues from

(G and H) Quantification of Z-disk width (G) and aspect ratio (H) of control- and *Parvb*-siRNA NRVCs. Data are shown as mean ± SEM from n = 4 independent biological replicates with 20–25 cells per group/replicate. ***$p < 0.001$, ****$p < 0.0001$, Student's t test.

(I) Confocal micrographs showing vinculin immunofluorescence and GFP-fluorescence in control-siRNA NRVCs expressing GFP or GFP-β-parvin. Note colocalization of GFP-β-parvin, but not GFP with vinculin. Scale bars, 5 μm.

(J) Confocal micrographs of vinculin immunofluorescence and DRAQ5-staining in control- and *Parvb*-siRNA NRVCs. Scale bars, 5 μm.

(K) Bright field micrographs of 3D cardiac microtissues from control- and *Parvb*-siRNA-treated NRVCs three days after tissue formation. Scale bars, 250 μm.

(L–N) Quantification of contractile force generation (L), time from contraction onset to force peak (M), and force relaxation time (N) of 3D cardiac microtissues from control- and *Parvb*-siRNA-treated NRVCs. Data are shown as mean ± SEM from n = 3 independent biological replicates with 12–17 tissues per group/replicate. *$p < 0.05$, **$p < 0.01$, Student's t test.

See also Figure S3 and Videos S1, S2, and S3.

Please cite this article in press as: Thievessen et al., The focal adhesion protein β-parvin controls cardiomyocyte shape and sarcomere assembly in response to mechanical load, Current Biology (2022), https://doi.org/10.1016/j.cub.2022.05.047

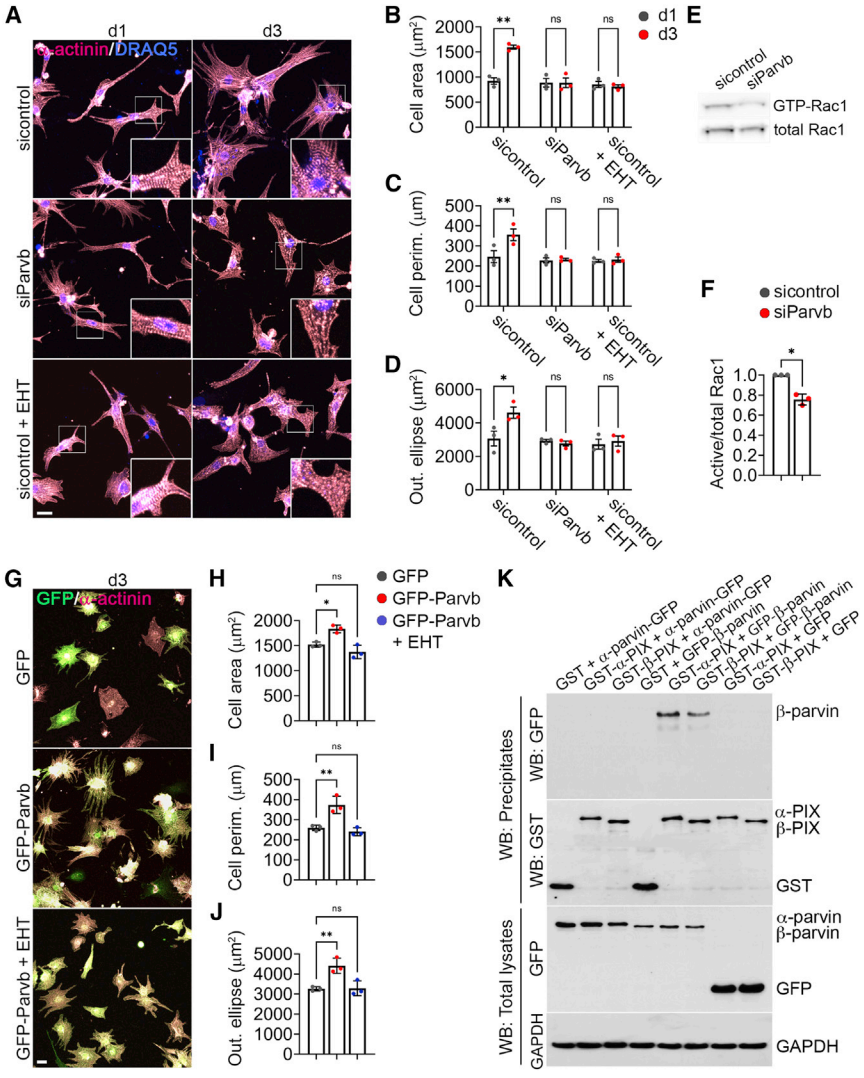

Figure 3. β-parvin-mediated Rac1-activation induces growth of SCPs and NRVCs

(A) Confocal micrographs showing α-actinin immunofluorescence and DRAQ5-staining of NRVCs transfected with control- and *Parvb*-siRNA, as well as NRVCs transfected with control-siRNA after treatment with 20 μM Rac-inhibitor EHT1864. Note increased cell size, well-organized α-actinin striation (inserts), and long α-actinin positive cell protrusions in control- but not *Parvb*-siRNA or control-siRNA EHT1864 NRVCs. Scale bars, 20 μm.

(B–D) Quantification of cell area (B), cell perimeter (C), and outer bounding ellipse area (D) of control- and *Parvb*-siRNA NRVCs, as well as EHT1864-treated control-siRNA NRVCs. Data are shown as mean ± SEM from n = 3 independent biological replicates with 48–157 cells per group/replicate. ns, $p > 0.05$; *$p < 0.05$, **$p < 0.01$.

(E) Western blot analysis of lysates from control- and *Parvb*-siRNA NRVCs after Rac1 pull-down.

(F) Densitometry-based quantification of (E); mean ± SD from n = 3 independent biological replicates. *p = 0.016, Student's t test.

(G) Confocal micrographs showing α-actinin immuno- and GFP-fluorescence of NRVCs expressing GFP or GFP-tagged β-parvin in the absence or presence of 20 μM Rac-inhibitor EHT1864. Note EHT1864-mediated block of GFP-β-parvin-induced increase in cell area and the size of α-actinin positive cell protrusions. Scale bars, 20 μm.

(H–J) Quantification of cell area (H), cell perimeter (I), and outer bounding ellipse area (J) of control- and *Parvb*-siRNA NRVCs, as well as EHT1864-treated control-siRNA NRVCs. Data are shown as mean ± SEM from n = 3 independent biological replicates with 80–178 cells per group/replicate. ns, $p > 0.05$; *$p < 0.05$, **$p < 0.01$.

(K) Western blot analysis of GST-PIX, parvin-GFP and GAPDH levels after GST pull-down and in total cell lysates, taken 24 h after co-transfection of the indicated GST-PIX and parvin-GFP expression constructs in COS cells. Note co-precipitation of β-parvin (top, lanes 5+6) but not α-pavin (top, lanes 2+3) with both α- and β-PIX (2nd panel). GFP and GAPDH of total lysates served as control for protein input; 20 μL of total lysates and GST-precipitates were loaded per lane.

See also Figure S4.

control and *Parvb*-siRNA NRVCs, suggesting that the contraction proceeds normally in the absence of β-parvin (Figures 2M and 2N). Altogether, our findings demonstrate that β-parvin triggers a signaling pathway in integrin-based cell-ECM adhesions of NRVCs whose signaling output includes serial sarcomere assembly, cell edge protrusion, dynamic growth of SCPs, adhesion site formation, and cardiomyocyte contractility.

β-parvin promotes SCP formation and increases NRVC surface area by activating Rac1

The reorganization of the actin cytoskeleton resulting in the formation of membrane protrusions requires the activities of small RhoA-like GTPases including Rac1.[43,54,55] Since β-parvin was shown to activate Rac1 via the Rac1/Cdc42-guanine nucleotide exchange factors (GEF) PIX in C2C12 cells,[56,57] we tested whether the β-parvin-mediated expansion of the NRVC surface area also operates via Rac1 by chemically inhibiting Rac1 activity with EHT1864 in control-siRNA NRVCs.[58] Similar to the loss of β-parvin in NRVCs, EHT1864 treatment inhibited the increase in cell area, cell perimeter, and outer bounding ellipse area (Figures 3A–3D) suggesting that the increase of the NRVC surface area and SCP growth are Rac1 dependent. This conclusion was supported by GTP-Rac pull-down assays, which revealed a significant reduction of GTP-bound to total Rac1 levels in *Parvb*- compared with control-siRNA NRVCs (Figures 3E and 3F). Furthermore, EHT1864-treatment also inhibited the growth of SCPs and the expansion of the NRVC surface area induced by β-parvin overexpression (Figures 3G–3J). In line with these findings, overexpression of the dominant-negative GFP-Rac1-T17N cDNA reduced surface area, perimeter, and outer bounding ellipse area of NRVCs compared with non-transfected control NRVCs (Figures S4A–S4D). Conversely, overexpression of the constitutively active

Please cite this article in press as: Thievessen et al., The focal adhesion protein β-parvin controls cardiomyocyte shape and sarcomere assembly in response to mechanical load, Current Biology (2022), https://doi.org/10.1016/j.cub.2022.05.047

CellPress

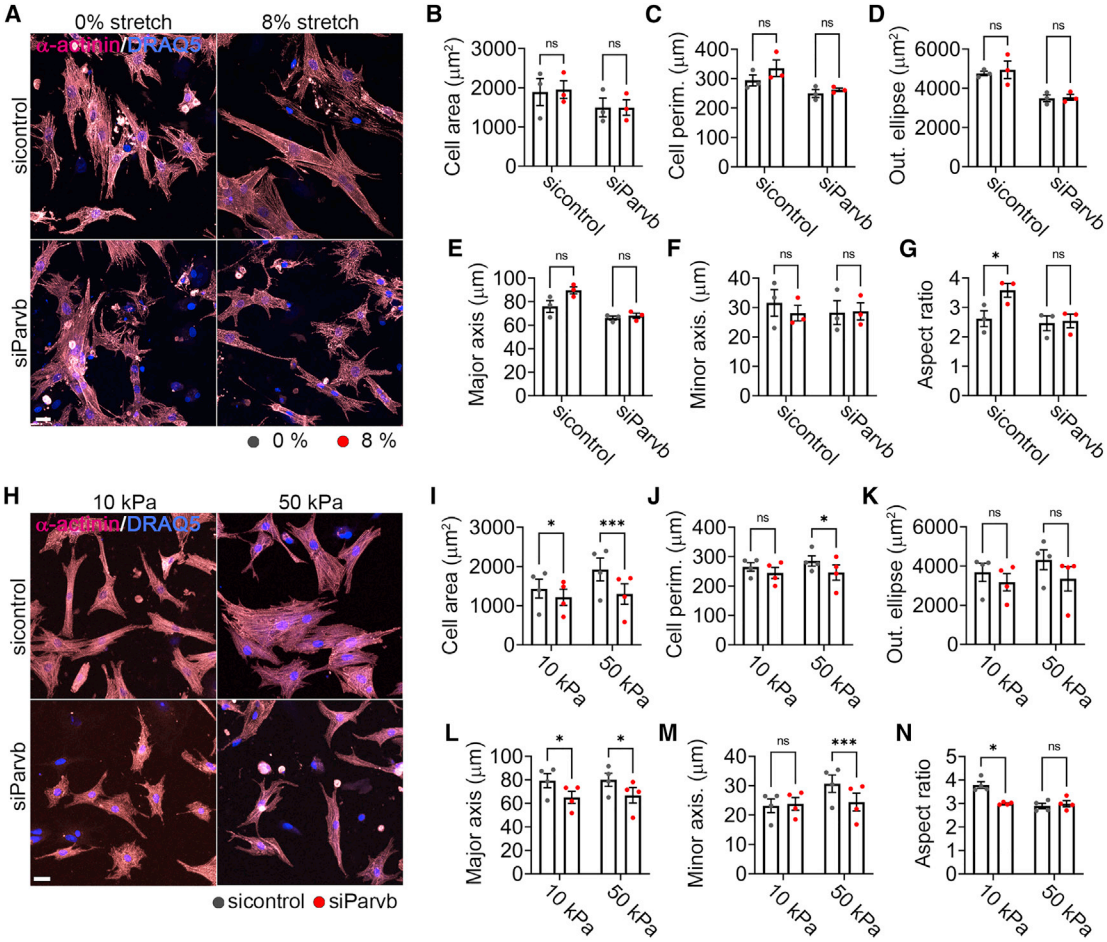

Figure 4. β-parvin is required for cyclic stretch and physiological substrate stiffness induced longitudinal growth of NRVCs

(A) Confocal micrographs showing α-actinin immunofluorescence and DRAQ5-staining of control- and *Parvb*-siRNA NRVCs subjected for 48 h to uni-axial cyclic stretch (8%, 1 Hz). Scale bars, 20 µm.

(B–G) Quantification of cell area (B), cell perimeter (C), outer bounding ellipse (D), major axis (E), minor axis (F), and aspect ratio (G) of stretched and non-stretched control- and *Parvb*-siRNA NRVCs. Data are shown as mean ± SEM from n = 3 independent biological replicates with 78–160 cells per group/replicate. ns, $p > 0.05$; *$p < 0.05$.

(H) Confocal micrographs showing α-actinin immunofluorescence and DRAQ5-staining of control- and *Parvb*-siRNA NRVCs on d3 of culture on collagen I coated polyacrylamide-substrates at indicated stiffness. Note elongated shape of control- compared with *Parvb*-siRNA NRVCs at 10 kPa substrate stiffness. Scale bars, 20 µm.

(I–N) Quantification of cell area (I), cell perimeter (J), outer bounding ellipse (K), major axis (L), minor axis (M), and aspect ratio (N) of control- and *Parvb*-siRNA NRVCs cultured on collagen I coated polyacrylamide-substrates at indicated stiffness. Data are shown as mean ± SEM from n = 4 independent biological replicates with 51–265 cells per group/replicate. ns, $p > 0.05$; *$p < 0.05$, ***$p < 0.001$.

See also Figure S5.

GFP-Rac1-Q61L cDNA increased the surface area of NRVCs and induced an excessive formation of lamellipodia (Figures S4A–S4D). Finally, we also found that the Rac1-GEF PIX-proteins co-immunoprecipitated with β-parvin but not with α-parvin (Figure 3K, lanes 2–3 and 5–6), which may explain why Rac1 activation and NRVC spreading were not compensated by α-parvin (Figures 1H–1K).

Physiological mechanical load induces cardiomyocyte elongation via β-parvin

The assembly of newly synthesized sarcomeres either in series or in parallel to existing ones determines the shape of hypertrophic cardiomyocytes and whether the heart responds with physiological or pathological hypertrophic growth *in vivo*.[1,2] Since cardiomyocytes undergo cycles of contraction and relaxation *in vivo*, we investigated whether β-parvin influences the spreading area and morphology of NRVCs under conditions of increased passive elongation induced by the application of cyclic, uni-axial stretch (8%, 1 Hz) for 48 h.[59,60] Neither control- nor *Parvb*-siRNA NRVCs responded to stretch by further increasing cell area, perimeter, or outer bound ellipse area (Figures 4A–4D). However, control-siRNA NRVCs showed a tendency to increase cell length (major axis) and decrease cell width (minor axis), resulting in a significantly increased aspect ratio (Figures 4A and 4E–4G). The absence of this cell morphology response in *Parvb*-siRNA NRVCs (Figures 4A and 4E–4G)

Please cite this article in press as: Thievessen et al., The focal adhesion protein β-parvin controls cardiomyocyte shape and sarcomere assembly in response to mechanical load, Current Biology (2022), https://doi.org/10.1016/j.cub.2022.05.047

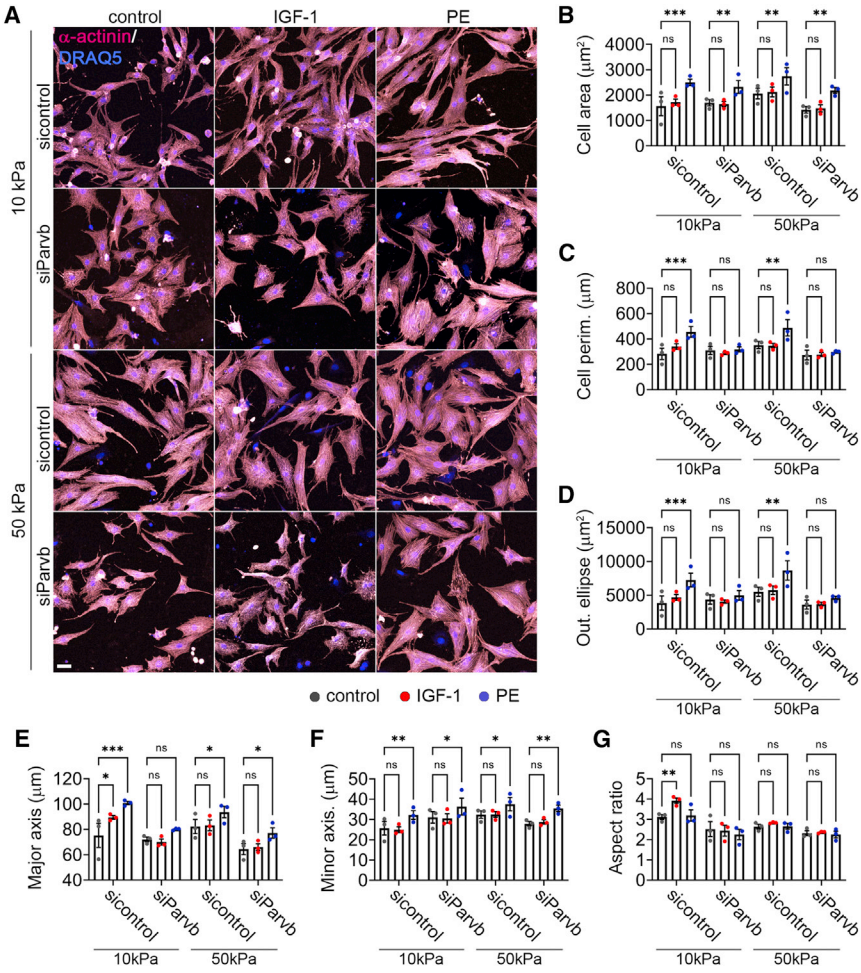

Figure 5. IGF-1- and PE-induced longitudinal growth of NRVCs at physiological substrate stiffness requires β-parvin

(A) Confocal micrographs showing α-actinin immunofluorescence and DRAQ5-staining of untreated, IGF-1-treated, and PE-treated control- and *Parvb*-siRNA NRVCs cultured on collagen I coated polyacrylamide-substrates at indicated stiffness. Note elongated shape of control- compared to *Parvb*-siRNA NRVCs at 10 kPa substrate stiffness in the presence of IGF-1. Scale bars, 20 μm.

(B–G) Quantification of cell area (B), cell perimeter (C), outer bounding ellipse (D), major axis (E), minor axis (F), and aspect ratio (G) of control- and *Parvb*-siRNA NRVCs cultured on collagen I coated polyacrylamide-substrates at indicated stiffness. Data are shown as mean ± SEM from n = 3 independent biological replicates with 69–204 cells per group/replicate. ns, $p > 0.05$; *$p < 0.05$, **$p < 0.01$, ***$p < 0.001$.

See also Figure S6.

IGF-1 and phenylephrine induce cardiomyocyte elongation at physiological substrate stiffness through the β-parvin-Rac1 signaling axis

To test whether β-parvin also regulates the morphology of NRVCs in response to hypertrophic agonists at different substrate stiffnesses, we stimulated NRVCs cultured on 10 and 50 kPa substrates, respectively, with insulin-like growth factor-1 (IGF-1) or phenylephrine (PE), which trigger physiological and pathological cardiac hypertrophy, respectively.[6,7,53] The treatment with PE induced an increase in cell area on 10 as well as 50 kPa stiff substrates in both, control- and *Parvb*-siRNA NRVCs (Figures 5A–5D) suggesting that despite the smaller cell area of *Parvb*- versus control-siRNA NRVCs seeded on 50 kPa substrates or collagen-coated glass (Figures 1, 2, 3, and S6A–S6C), PE-induced NRVC hypertrophy proceeds in a β-parvin independent manner. Consistent with the requirement of β-parvin for SCP growth and NRVC elongation (Figures 2 and 4), the PE-induced increase in cell area in *Parvb*-siRNA NRVCs was not associated with an increase in cell perimeter, outer bounding ellipse area or cell length, but with an increase in cell width (Figures 5A–5F). Interestingly, IGF-1 treatment of control- or *Parvb*-siRNA NRVCs affected neither cell area, perimeter, nor outer bounding ellipse area on 10 or 50 kPa stiff substrates. However, IGF-1- as well as PE-treated control-siRNA NRVCs increased cell length but not width on 10 kPa substrates, resulting in an increased aspect ratio, which was absent in *Parvb*-siRNA NRVCs seeded on 10 kPa stiff substrates (Figures 5A, 5E–5G, and S6D–S6F). In contrast, on 50 kPa substrates both IGF-1- and PE-treatment moderately and comparably increased cell length of control- and *Parvb*-siRNA NRVCs without affecting the aspect ratio (Figures 5A, 5E–5G, and S6D–S6F). Altogether, these findings show that different

indicates that the cyclic, uni-axial stretch-induced, elongated shape of normal cardiomyocytes is accomplished by β-parvin. In our second experimental setup, we tested whether β-parvin also shapes the mechano-response of NRVCs cultured on compliant substrates of physiological stiffness. Based on published data showing that the Young's modulus of healthy striated muscle tissue is approximately 10 kPa[61,62] and of pressure-overloaded, pathological myocardial tissue up to 7-fold higher than volume-overloaded, physiological myocardial tissue,[63] we performed our experiments on collagen I coated polyacrylamide (PAA) substrates with Young's moduli of 10 and 50 kPa, respectively. Control- and *Parvb*-siRNA NRVCs significantly increased cell area, perimeter, and outer bounding ellipses at 10 as well 50 kPa substrate stiffness, although the increase of these parameters was stronger in control-siRNA NRVCs (Figures 4H–4K and S5A–S5D). Amazingly, control-siRNA NRVCs grew on 10 kPa substrates mainly in length and on 50 kPa substrates to the same extent in width and length. The length growth on 10 kPa substrates resulted in an increase of the aspect ratio of control-siRNA NRVCs (Figures 4H and 4L–4N), which was absent in *Parvb*-siRNA NRVCs (Figures 4H and 4L–4N). These findings indicate that β-parvin is required for cardiomyocyte elongation in response to physiological mechanical stimuli such as cyclic strain or substrate compliance.

Please cite this article in press as: Thievessen et al., The focal adhesion protein β-parvin controls cardiomyocyte shape and sarcomere assembly in response to mechanical load, Current Biology (2022), https://doi.org/10.1016/j.cub.2022.05.047

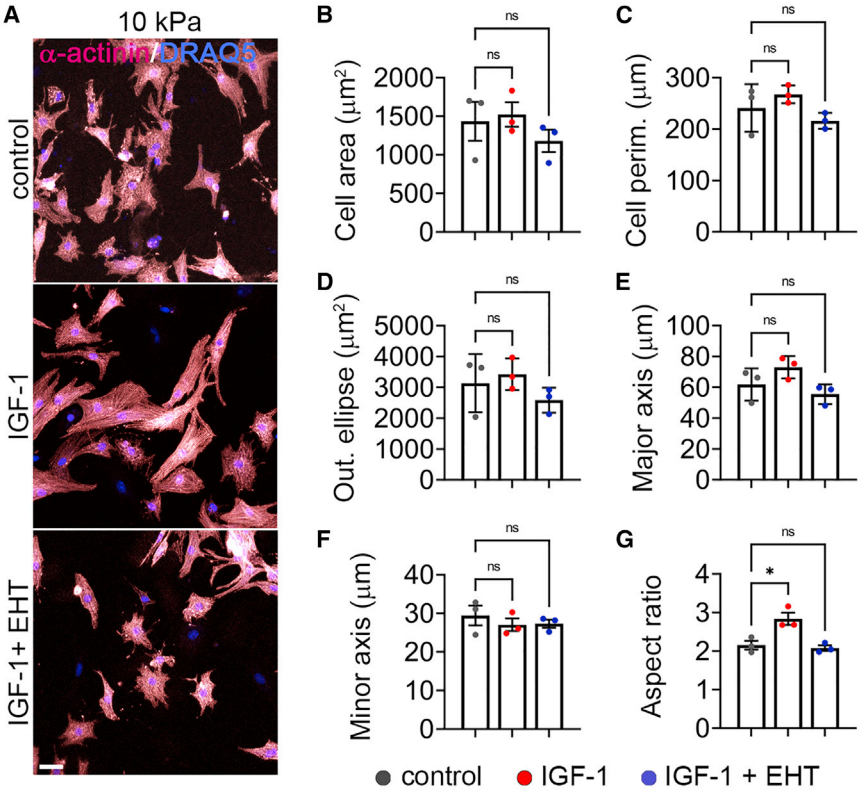

Figure 6. IGF-1-induced longitudinal growth of NRVCs at physiological substrate stiffness requires Rac1 activation

(A) Confocal micrographs showing α-actinin immunofluorescence and DRAQ5 staining of untreated, IGF-1-treated, and IGF-1 + EHT1864-treated NRVCs cultured on collagen I coated polyacrylamide-substrates of 10 kPa Young's modulus. Note elongated shape of IGF-1-treated compared to untreated or IGF-1 + EHT1864-treated NRVCs. Scale bars, 20 μm.

(B–G) Quantification of cell area (B), cell perimeter (C), outer bounding ellipse (D), major axis (E), minor axis (F), and aspect ratio (G) of untreated, IGF-1-treated, and IGF-1 + EHT1864-treated NRVCs cultured on collagen I coated polyacrylamide-substrates at 10 kPa substrate stiffness. Data are shown as mean ± SEM from n = 3 independent biological replicates with 45–146 cells per group/replicate. ns, $p > 0.05$; *$p < 0.05$.

(H) Western blot analysis of phospho-serine-473 and total PKB/Akt levels in control- and *Parvb*-siRNA NRVCs on d3 of culture on collagen I coated polyacrylamide-substrates of 10 kPa Young's modulus without (lanes 1 and 2) and after 30 min stimulation with IGF-1 (lanes 3 and 4).

(I) Densitometry-based quantification of (H); mean ± SD from n = 3 independent biological replicates. ns, $p > 0.05$, Student's t test.

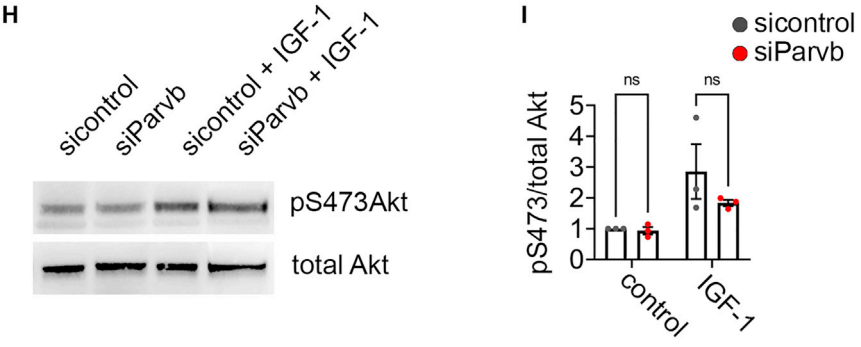

hypertrophic agonists induce NRVC elongation at physiological substrate stiffness via β-parvin.

Next, we tested whether β-parvin-mediated NRVC elongation at physiological substrate stiffness occurs via Rac1 by treating NRVCs on 10 kPa substrates with IGF-1 supplemented with or without EHT1864. The experiments revealed that the IGF-1-induced increase in NRVC aspect ratio was blocked by EHT1864 (Figures 6A–6G), indicating that IGF-1-induced NRVC hypertrophy at physiological substrate stiffness is mediated by β-parvin-Rac1-induced NRVC elongation. Since IPP complexes were shown to regulate cardiomyocyte hypertrophy by activating protein kinase-B (PKB)/Akt, we tested whether loss of β-parvin affects basal and/or IGF-1 induced PKB/Akt activity. Contrary to our expectation, western blot analyses revealed comparable total and phospho-serine 473 PKB/Akt levels in control- and *Parvb*-siRNA NRVCs cultured on 10 kPa substrates and treated with or without IGF-1 for 30 min (Figures 6H and 6I).

β-parvin is required for volume-overload-induced cardiac hypertrophy *in vivo*

To test β-parvin functions *in vivo*, we ablated the *Parvb* gene in the germline of mice (Figure S7A). *Parvb*$^{-/-}$ mice lacked *Parvb* mRNA and protein (Figures S7B, S7E, and S7F), were viable, and were without overt defects (Figures S7C and S7D). Echocardiographic and morphometric measurements revealed regular myocardial morphology, normal heart/body weight ratio, left ventricular mass, cardiomyocyte diameter, and capillary-to-myocyte ratio in 4-month-old *Parvb*$^{-/-}$ mice under basal conditions (Figures 7A–7D; Table S2). Ejection fraction and left ventricular end-diastolic and end-systolic volumes were also unaffected in *Parvb*$^{-/-}$ hearts (Figures 7E–7G) indicating that *Parvb*$^{-/-}$ mice have normal cardiac function under basal conditions. Notably, lysates of *Parvb*$^{-/-}$ hearts had elevated α-parvin and normal ILK protein levels (Figures S7B and S7F), indicating that β-parvin protein loss led to increased assembly of α-parvin-containing IPP complexes that compensated for β-parvin loss in the developing and unstressed, postnatal heart. Importantly, however, *Parvb*$^{-/-}$ neonatal mouse ventricular cardiomyocytes (NMVCs) cultured on collagen (Figures 7H–7L) phenocopied the punctate α-actinin pattern, the reduced cell area, and diminished aspect ratio of *Parvb*-siRNA-treated NRVCs (see Figures 1C–1G and 4).

Next, we exposed control and *Parvb*$^{-/-}$ mice to pressure-overload that triggers pathological cardiac hypertrophy. Transverse aortic constriction (TAC) for 3 weeks increased ECM

Please cite this article in press as: Thievessen et al., The focal adhesion protein β-parvin controls cardiomyocyte shape and sarcomere assembly in response to mechanical load, Current Biology (2022), https://doi.org/10.1016/j.cub.2022.05.047

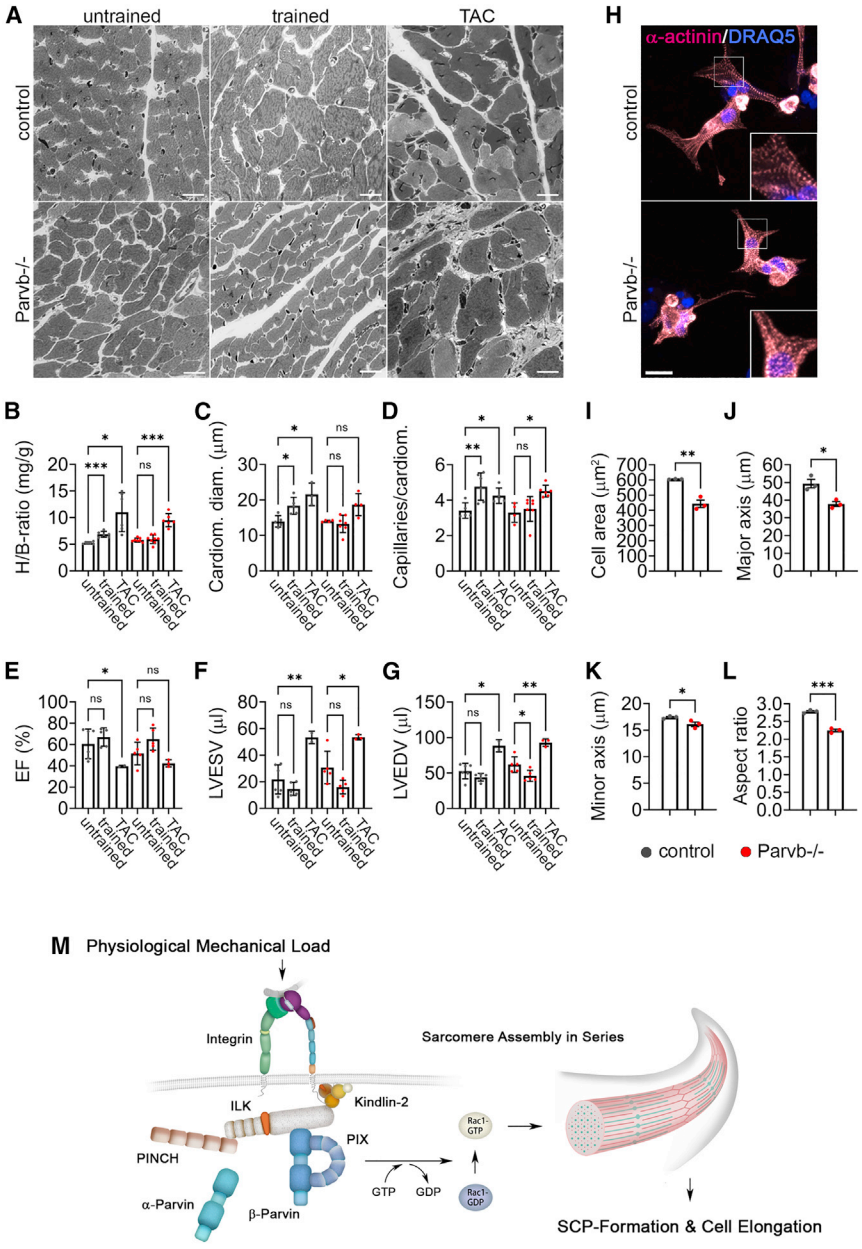

Figure 7. β-parvin requirement for volume-overload-induced cardiac hypertrophy in mice

(A) Electronmicrographs of left ventricular tissue of 3- to 6-month-old control and *Parvb*$^{-/-}$ mice under sedentary conditions, after 4 weeks of forced treadmilling exercise (trained) or 3 weeks of *trans*-aortic constriction (TAC). Scale bars, 25 μm.

(B–D) Heart/body (H/B)-weight ratio (B), cardiomyocyte diameter (C), and capillarization (D) in left ventricular tissue of sedentary, trained, and TAC control and *Parvb*$^{-/-}$ mice.

(E–G) Ejection fraction (EF) (E), left ventricular end-diastolic (LVEDV) (F), and end-systolic volumina (LVESV) (G) in sedentary, trained, and TAC control and *Parvb*$^{-/-}$ mice. Data are shown as mean ± SEM from n = 2–7 mice per group. ns, $p > 0.05$; *$p < 0.05$, **$p < 0.01$, ***$p < 0.001$, Student's t test.

(H) Confocal micrographs showing α-actinin immunofluorescence and DRAQ5-staining of control and *Parvb*$^{-/-}$ NMVCs after 4 days in culture. Note reduced size and aspect ratio, and punctate α-actinin striation in *Parvb*$^{-/-}$ compared with control NMVCs. Scale bars, 20 μm.

(I–L) Quantification of cell area (I), major axis (J), minor axis (K), and aspect ratio (L) of control and *Parvb*$^{-/-}$ NMVCs. Data are shown as mean ± SEM from n = 3 independent biological replicates with 18–69 cells per group/replicate. *$p < 0.05$, **$p < 0.01$, ***$p < 0.001$.

(M) Working model for the role of β-parvin in physiological cardiac hypertrophy. In response to exercise-induced volume overload, β-parvin associates with α/β-PIX, which activates Rac1 followed by membrane protrusion and the assembly of newly synthesized sarcomeres in series to existing ones, resulting in cardiomyocyte elongation and adaptive hypertrophic growth of the heart.

See also Figure S7 and Table S2.

depositions, heart/body weight ratio, left ventricular mass, cardiomyocyte diameter, and number of capillaries per myocyte to the same extent in control and *Parvb*$^{-/-}$ hearts (Figures 7A–7D; Table S2). TAC-treated control and *Parvb*$^{-/-}$ animals displayed reduced left ventricular function compared with their sedentary counterparts, as shown by a decreased ejection fraction accompanied by a significant increase in end-systolic and end-diastolic volumes (Figures 7E–7G), which altogether indicates that β-parvin is not required for the response to pressure-overload in mice.

To test the response to physiological mechanical load, we challenged control and *Parvb*$^{-/-}$ mice with a daily, forced treadmill exercise over a period of four weeks. Exercised control mice showed an increase in heart/body weight ratio, cardiomyocyte diameter, and capillarization when compared with sedentary control mice (Figures 7A–7D). In contrast, *Parvb*$^{-/-}$ mice failed to increase heart/body weight ratio, cardiomyocyte diameter, and capillarization upon exercise (Figures 7A–7D). Most cardiac functions remained normal in trained *Parvb*$^{-/-}$ mice (Figures 7E and 7F; Table S2), whereas left ventricular end-diastolic volume was reduced in exercised *Parvb*$^{-/-}$ but not control hearts (Figure 7G). These data demonstrate that β-parvin is also required to induce hypertrophic growth of the heart in response to volume-overload *in vivo*.

DISCUSSION

Cardiomyocytes have the remarkable ability to sense and discriminate between different mechanical cues and respond with a characteristic cell size increase (hypertrophy) and assembly of new sarcomeres. The response to exercise-induced volume-overload is primarily characterized by a longitudinal cell growth and predominantly serial arrangements of new sarcomeres resulting in a reversible and physiological cardiac

Please cite this article in press as: Thievessen et al., The focal adhesion protein β-parvin controls cardiomyocyte shape and sarcomere assembly in response to mechanical load, Current Biology (2022), https://doi.org/10.1016/j.cub.2022.05.047

adaption to the mechanical stress, whereby the geometric proportions of the heart ventricles remain unaffected. By contrast, the response to pressure overload due to, e.g., hypertension leads to lateral cell growth and the parallel arrangements of new sarcomeres, resulting in an irreversible thickening of the ventricular wall muscle. The profoundly different response to different mechanical stresses points to the existence of different sensing and signaling systems that orchestrate the different shape changes and sarcomere assemblies. In search for cardiac mechanosensors, several laboratories reported that β1-class integrins play a central role in inducing cardiac hypertrophy *in vitro* and *in vivo*.[26,28,64,65] Since β1 integrins recruit numerous mechanosensitive proteins to adhesion sites,[66,67] we searched for highly expressed integrin-associated adhesion proteins and protein complexes in the heart muscle and tested their role for mechanical stress-specific responses. In the present study, we identified β-parvin as novel mechano-responsive adhesion protein in costameres and show that β-parvin is required for serial sarcomere assembly and elongated growth of hypertrophic cardiomyocytes *in vitro* and for volume-overload-induced cardiac hypertrophy *in vivo*.

Our proteomics screen for cardiac-enriched integrin adhesion-associated proteins identified particularly high levels of β-parvin in the cardiomyocyte proteome. Functional studies with *in vitro* cultured β-parvin-depleted NRVCs and β-parvin-null NMVCs revealed that β-parvin is required for longitudinal cardiomyocyte growth and growth of sarcomere-containing protrusions (SCPs) under conditions mimicking cardiac preload *in vitro*, such as culturing NRVCs on collagen substrates with physiological rigidity or exposing NRVCs to eccentric loading by applying cyclic, uni-axial stretch. Furthermore, both IGF-1- and PE-treatment of NRVCs induced longitudinal cell growth in a β-parvin-dependent manner on physiologically stiff 2D-substrates and not on 2D-substrates of pathologically high rigidity. The signaling pathway activated downstream of β-parvin commences with the recruitment of α- and β-PIX followed by the activation of Rac1 and concludes with serial assemblies of sarcomeres and elongated growth of cardiomyocytes (Figure 7M). Our findings showing that α-parvin does not bind to α- and β-PIX provide a rational explanation why α-parvin is unable to compensate the loss of β-parvin in cardiomyocytes in our *in vitro* and *in vivo* experiments. The high degree of sequence and structural homology between parvin isoforms makes it difficult to predict where α-/β-PIX mediates the interaction with β-parvin. Although the N terminus is least conserved among the parvins and contains isoform-specific serine/threonine-phosphorylation sites,[68–70] overexpression of β-parvin fragments in HeLa cells identified the CH1-domain responsible for Rac1-dependent lamellipodium formation via α-/β-PIX.[71]

Our *in vivo* experiments confirm the *in vitro* data and demonstrate that *Parvb*$^{-/-}$ mice, which develop without apparent defects, failed to induce a cardiac hypertrophy response to forced treadmill exercise/volume-overload. This finding indicates that the ILK/PINCH/β-parvin complex serves as volume load-specific mechano-responsive complex at cardiomyocyte/ECM adhesion sites *in vivo* that promotes physiological hypertrophy. Consistent with our *in vitro* data, this functional property of the ILK/PINCH/β-parvin complex is not compensated by the ILK/PINCH/α-parvin complex, which plays an indispensable role during development by facilitating the septation of the cardiac outflow tract and the formation and/or stabilization of cardiac sarcomeres.[40]

The normal cardiac development and response to TAC-induced pressure-overload in the absence of β-parvin is surprising, considering its requirement for NRVC areal expansion *in vitro*. This could be due to different effects of the cardiomyocyte microenvironment under cardiac pressure and volume-overload conditions *in vivo*, where the cells adhere through costameres across the whole cell surface, as opposed to stiff versus soft 2D culture substrates, where the cells form a small, ventrally located cell adhesion area. Pathological cardiac hypertrophy is furthermore associated with the reactivation of fetal gene expression,[1] which our *in vitro* culture may not be able to reproduce. We can also not exclude functional redundancy or compensation by α-parvin under TAC conditions. Parvin isoforms have the ability to provide the IPP complex with specific functions. It has been shown, for example, that ILK-dependent PKB/Akt activation is mediated by β-parvin in zebrafish cardiomyocytes[42] and by α-parvin in dilated cardiomyopathy of human patients as well as in murine aortic banding- and myocardial infarction models.[72] It clearly requires more studies to assign specific functions to distinct IPPs and determine which are shared due to redundancy or compensatory upregulation of IPP complexes.

STAR★METHODS

Detailed methods are provided in the online version of this paper and include the following:

- KEY RESOURCES TABLE
- RESOURCE AVAILABILITY
  - Lead contact
  - Materials availability
  - Data and code availability
- EXPERIMENTAL MODEL AND SUBJECT DETAILS
  - Animals
  - Isolation and culture of NRVC/NMVC
  - HEK293T cells
- METHOD DETAILS
  - Heart proteome analysis
  - siRNA-mediated knockdown of Parvb in NRVCs
  - Viral expression of murine α- and β-parvin in NRVCs
  - Transient expression of skeletal muscle tropomyosin-GFP and GFP-Rac1-Q61L/T17N in NRVCs
  - NRVC culture on flexible polyacrylamide substrates
  - Uni-axial stretching of NRVCs on 2D PDMS membranes
  - Spinning disk adhesion assay
  - Generation of 3D cardiac microtissues and quantification of forces
  - Microscopy and morphological analysis of NRVCs/NMVCs
  - Generation of Parvb$^{-/-}$ mice
  - Echocardiography
  - Electron Microscopy
  - Histology and immunohistochemistry
  - Western and Northern Blots

- Rac1 activation assay and GST-PIX pull-down/parvin-GFP co-precipitation
- Antibodies
- QUANTIFICATION AND STATISTICAL ANALYSIS
  - Statistical analysis

SUPPLEMENTAL INFORMATION

Supplemental information can be found online at https://doi.org/10.1016/j.cub.2022.05.047.

ACKNOWLEDGMENTS

The authors thank Mojgan Gilhav, Bianca Collins, and Anika Voss for technical assistance; Julia Kraxner for help developing the microtissue model; Dr. Markus Moser for help with *in situ* hybridization; and Drs. Roy Zent and Arnoud Sonnenberg for critically reading the manuscript. The work was funded by the DFG (SFB-863-Project B3), European Research Council (grant agreement no. 810104—Point), and the Max Planck Society.

AUTHOR CONTRIBUTIONS

Conceptualization, I.T., R.F., and W.B.; methodology, I.T., W.B., B.F., and R.F.; software, B.F.; investigation, I.T., S.V., R.T.B., F.S., G.R., O.D., A.G., and M.K.; resources, R.F., B.F., and F.B.E.; writing, I.T. and R.F.; visualization, I.T., F.S., and R.T.B.; supervision, R.F., W.B., B.F., B.K.F., and K.B.; project administration, R.F. and I.T.; funding acquisition, R.F.

DECLARATION OF INTERESTS

The authors declare no competing interests.

Received: December 1, 2021
Revised: April 12, 2022
Accepted: May 17, 2022
Published: June 9, 2022

REFERENCES

1. Nakamura, M., and Sadoshima, J. (2018). Mechanisms of physiological and pathological cardiac hypertrophy. Nat. Rev. Cardiology *15*, 387–407. https://doi.org/10.1038/s41569-018-0007-y.
2. Russell, B., Curtis, M.W., Koshman, Y.E., and Samarel, A.M. (2010). Mechanical stress-induced sarcomere assembly for cardiac muscle growth in length and width. J. Mol. Cell. Cardiol. *48*, 817–823. https://doi.org/10.1016/j.yjmcc.2010.02.016.
3. Nagai, T., Tanaka-Ishikawa, M., Aikawa, R., Ishihara, H., Zhu, W., Yazaki, Y., Nagai, R., and Komuro, I. (2003). Cdc42 plays a critical role in assembly of sarcomere units in series of cardiac myocytes. Biochem. Biophys. Res. Commun. *305*, 806–810.
4. Maillet, M., van Berlo, J.H., and Molkentin, J.D. (2013). Molecular basis of physiological heart growth: fundamental concepts and new players. Nat. Rev. Mol. Cell Biol. *14*, 38–48. https://doi.org/10.1038/nrm3495.
5. Wollert, K.C., Taga, T., Saito, M., Narazaki, M., Kishimoto, T., Glembotski, C.C., Vernallis, A.B., Heath, J.K., Pennica, D., Wood, W.I., and Chien, K.R. (1996). Cardiotrophin-1 activates a distinct form of cardiac muscle cell hypertrophy. Assembly of sarcomeric units in series VIA gp130/leukemia inhibitory factor receptor-dependent pathways. J. Biol. Chem. *271*, 9535–9545.
6. McMullen, J.R., Shioi, T., Huang, W.Y., Zhang, L., Tarnavski, O., Bisping, E., Schinke, M., Kong, S., Sherwood, M.C., Brown, J., et al. (2004). The insulin-like growth factor 1 receptor induces physiological heart growth via the phosphoinositide 3-kinase(p110α) pathway. J. Biol. Chem. *279*, 4782–4793. https://doi.org/10.1074/jbc.M310405200.
7. McMullen, J.R., Shioi, T., Zhang, L., Tarnavski, O., Sherwood, M.C., Kang, P.M., and Izumo, S. (2003). Phosphoinositide 3-kinase(p110α) plays a critical role for the induction of physiological, but not pathological, cardiac hypertrophy. Proc. Natl. Acad. Sci. USA *100*, 12355–12360. https://doi.org/10.1073/pnas.1934654100.
8. Xie, J., He, G., Chen, Q., Sun, J., Dai, Q., Lu, J., Li, G., Wu, H., Li, R., Chen, J., et al. (2016). Syndecan-4 signaling is required for exercise-induced cardiac hypertrophy. Mol. Med. *22*, 192–201. https://doi.org/10.2119/molmed.2015.00026.
9. Naskar, S., Datta, K., Mitra, A., Pathak, K., Datta, R., Bansal, T., and Sarkar, S. (2014). Differential and conditional activation of PKC-isoforms dictates cardiac adaptation during physiological to pathological hypertrophy. PLoS One *9*, e104711. https://doi.org/10.1371/journal.pone.0104711.
10. Buyandelger, B., Ng, K.E., Miocic, S., Piotrowska, I., Gunkel, S., Ku, C.H., and Knöll, R. (2011). MLP (muscle LIM protein) as a stress sensor in the heart. Pflugers Arch *462*, 135–142. https://doi.org/10.1007/s00424-011-0961-2.
11. De Windt, L.J., Lim, H.W., Bueno, O.F., Liang, Q., Delling, U., Braz, J.C., Glascock, B.J., Kimball, T.F., del Monte, F., Hajjar, R.J., and Molkentin, J.D. (2001). Targeted inhibition of calcineurin attenuates cardiac hypertrophy in vivo. Proc. Natl. Acad. Sci. USA *98*, 3322–3327. https://doi.org/10.1073/pnas.031371998.
12. Wilkins, B.J., Dai, Y.S., Bueno, O.F., Parsons, S.A., Xu, J., Plank, D.M., Jones, F., Kimball, T.R., and Molkentin, J.D. (2004). Calcineurin/NFAT coupling participates in pathological, but not physiological, cardiac hypertrophy. Circ. Res. *94*, 110–118. https://doi.org/10.1161/01.RES.0000109415.17511.18.
13. Bueno, O.F., De Windt, L.J., Tymitz, K.M., Witt, S.A., Kimball, T.R., Klevitsky, R., Hewett, T.E., Jones, S.P., Lefer, D.J., Peng, C.F., et al. (2000). The MEK1-ERK1/2 signaling pathway promotes compensated cardiac hypertrophy in transgenic mice. EMBO J *19*, 6341–6350. https://doi.org/10.1093/emboj/19.23.6341.
14. Chaanine, A.H., and Hajjar, R.J. (2011). AKT signalling in the failing heart. Eur. J. Heart Fail. *13*, 825–829. https://doi.org/10.1093/eurjhf/hfr080.
15. Frey, N., Barrientos, T., Shelton, J.M., Frank, D., Rütten, H., Gehring, D., Kuhn, C., Lutz, M., Rothermel, B., Bassel-Duby, R., et al. (2004). Mice lacking calsarcin-1 are sensitized to calcineurin signaling and show accelerated cardiomyopathy in response to pathological biomechanical stress. Nat. Med. *10*, 1336–1343. https://doi.org/10.1038/nm1132.
16. Naga Prasad, S.V., Esposito, G., Mao, L., Koch, W.J., and Rockman, H.A. (2000). Gβγ-dependent phosphoinositide 3-kinase activation in hearts with in vivo pressure overload hypertrophy. J. Biol. Chem. *275*, 4693–4698.
17. Wang, J., Liu, X., Arneja, A.S., and Dhalla, N.S. (1999). Alterations in protein kinase A and protein kinase C levels in heart failure due to genetic cardiomyopathy. Can. J. Cardiol. *15*, 683–690.
18. Zheng, M., Dilly, K., Dos Santos Cruz, J., Li, M., Gu, Y., Ursitti, J.A., Chen, J., Ross, J., Jr., Chien, K.R., Lederer, J.W., and Wang, Y. (2004). Sarcoplasmic reticulum calcium defect in Ras-induced hypertrophic cardiomyopathy heart. Am. J. Physiol. Heart Circ. Physiol. *286*, H424–H433. https://doi.org/10.1152/ajpheart.00110.2003.
19. Dai, Y., Luo, W., and Chang, J. (2018). Rho kinase signaling and cardiac physiology. Curr. Opin. Physiol. *1*, 14–20. https://doi.org/10.1016/j.cophys.2017.07.005.
20. Doerries, C., Grote, K., Hilfiker-Kleiner, D., Luchtefeld, M., Schaefer, A., Holland, S.M., Sorrentino, S., Manes, C., Schieffer, B., Drexler, H., and Landmesser, U. (2007). Critical role of the NAD(P)H oxidase subunit p47phox for left ventricular remodeling/dysfunction and survival after myocardial infarction. Circ. Res. *100*, 894–903. https://doi.org/10.1161/01.RES.0000261657.76299.ff.
21. Hoshijima, M. (2006). Mechanical stress-strain sensors embedded in cardiac cytoskeleton: Z disk, titin, and associated structures. Am. J. Physiol. Heart Circ. Physiol. *290*, H1313–H1325. https://doi.org/10.1152/ajpheart.00816.2005.

22. Pardo, J.V., Siliciano, J.D., and Craig, S.W. (1983). A vinculin-containing cortical lattice in skeletal muscle: transverse lattice elements ("costameres") mark sites of attachment between myofibrils and sarcolemma. Proc. Natl. Acad. Sci. USA *80*, 1008–1012.

23. Sit, B., Gutmann, D., and Iskratsch, T. (2019). Costameres, dense plaques and podosomes: the cell matrix adhesions in cardiovascular mechanosensing. J. Muscle Res. Cell Motil. *40*, 197–209. https://doi.org/10.1007/s10974-019-09529-7.

24. Clemente, C.F., Tornatore, T.F., Theizen, T.H., Deckmann, A.C., Pereira, T.C., Lopes-Cendes, I., Souza, J.R., and Franchini, K.G. (2007). Targeting focal adhesion kinase with small interfering RNA prevents and reverses load-induced cardiac hypertrophy in mice. Circ. Res. *101*, 1339–1348. https://doi.org/10.1161/CIRCRESAHA.107.160978.

25. DiMichele, L.A., Doherty, J.T., Rojas, M., Beggs, H.E., Reichardt, L.F., Mack, C.P., and Taylor, J.M. (2006). Myocyte-restricted focal adhesion kinase deletion attenuates pressure overload-induced hypertrophy. Circ. Res. *99*, 636–645. https://doi.org/10.1161/01.RES.0000240498.44752.d6.

26. Li, R., Wu, Y., Manso, A.M., Gu, Y., Liao, P., Israeli, S., Yajima, T., Nguyen, U., Huang, M.S., Dalton, N.D., et al. (2012). β1 integrin gene excision in the adult murine cardiac myocyte causes defective mechanical and signaling responses. Am. J. Pathol. *180*, 952–962. https://doi.org/10.1016/j.ajpath.2011.12.007.

27. Manso, A.M., Li, R., Monkley, S.J., Cruz, N.M., Ong, S., Lao, D.H., Koshman, Y.E., Gu, Y., Peterson, K.L., Chen, J., et al. (2013). Talin1 has unique expression versus talin 2 in the heart and modifies the hypertrophic response to pressure overload. J. Biol. Chem. *288*, 4252–4264. https://doi.org/10.1074/jbc.M112.427484.

28. Shai, S.Y., Harpf, A.E., Babbitt, C.J., Jordan, M.C., Fishbein, M.C., Chen, J., Omura, M., Leil, T.A., Becker, K.D., Jiang, M., et al. (2002). Cardiac myocyte-specific excision of the β1 integrin gene results in myocardial fibrosis and cardiac failure. Circ. Res. *90*, 458–464.

29. Zemljic-Harpf, A.E., Miller, J.C., Henderson, S.A., Wright, A.T., Manso, A.M., Elsherif, L., Dalton, N.D., Thor, A.K., Perkins, G.A., McCulloch, A.D., and Ross, R.S. (2007). Cardiac-myocyte-specific excision of the vinculin gene disrupts cellular junctions, causing sudden death or dilated cardiomyopathy. Mol. Cell. Biol. *27*, 7522–7537. https://doi.org/10.1128/MCB.00728-07.

30. Zhang, Z., Mu, Y., Veevers, J., Peter, A.K., Manso, A.M., Bradford, W.H., Dalton, N.D., Peterson, K.L., Knowlton, K.U., Ross, R.S., et al. (2016). Postnatal loss of Kindlin-2 leads to progressive heart failure. Circ. Heart Fail. *9*, e003129. https://doi.org/10.1161/CIRCHEARTFAILURE.116.003129.

31. Chen, H., Huang, X.N., Yan, W., Chen, K., Guo, L., Tummalapali, L., Dedhar, S., St-Arnaud, R., Wu, C., and Sepulveda, J.L. (2005). Role of the integrin-linked kinase/PINCH1/α-parvin complex in cardiac myocyte hypertrophy. Lab. Invest. *85*, 1342–1356. https://doi.org/10.1038/labinvest.3700345.

32. Legate, K.R., Montañez, E., Kudlacek, O., and Fässler, R. (2006). ILK, PINCH and parvin: the tIPP of integrin signalling. Nat. Rev. Mol. Cell Biol. *7*, 20–31. https://doi.org/10.1038/nrm1789.

33. Qin, J., and Wu, C. (2012). ILK: a pseudokinase in the center stage of cell-matrix adhesion and signaling. Curr. Opin. Cell Biol. *24*, 607–613. https://doi.org/10.1016/j.ceb.2012.06.003.

34. Huang, Y., Li, J., Zhang, Y., and Wu, C. (2000). The roles of integrin-linked kinase in the regulation of myogenic differentiation. J. Cell Biol. *150*, 861–872. https://doi.org/10.1083/jcb.150.4.861.

35. Widmaier, M., Rognoni, E., Radovanac, K., Azimifar, S.B., and Fässler, R. (2012). Integrin-linked kinase at a glance. J. Cell Sci. *125*, 1839–1843. https://doi.org/10.1242/jcs.093864.

36. Fukuda, T., Chen, K., Shi, X., and Wu, C. (2003). PINCH-1 is an obligate partner of integrin-linked kinase (ILK) functioning in cell shape modulation, motility, and survival. J. Biol. Chem. *278*, 51324–51333. https://doi.org/10.1074/jbc.M309122200.

37. LaLonde, D.P., Grubinger, M., Lamarche-Vane, N., and Turner, C.E. (2006). CdGAP associates with actopaxin to regulate integrin-dependent changes in cell morphology and motility. Curr. Biol. *16*, 1375–1385. https://doi.org/10.1016/j.cub.2006.05.057.

38. Zhang, Y., Chen, K., Tu, Y., and Wu, C. (2004). Distinct roles of two structurally closely related focal adhesion proteins, α-parvins and β-parvins, in regulation of cell morphology and survival. J. Biol. Chem. *279*, 41695–41705. https://doi.org/10.1074/jbc.M401563200.

39. Vaynberg, J., Fukuda, K., Lu, F., Bialkowska, K., Chen, Y., Plow, E.F., and Qin, J. (2018). Non-catalytic signaling by pseudokinase ILK for regulating cell adhesion. Nat. Commun. *9*, 4465. https://doi.org/10.1038/s41467-018-06906-7.

40. Montanez, E., Wickström, S.A., Altstätter, J., Chu, H., and Fässler, R. (2009). α-Parvin controls vascular mural cell recruitment to vessel wall by regulating RhoA/ROCK signalling. EMBO J. *28*, 3132–3144. https://doi.org/10.1038/emboj.2009.295.

41. White, D.E., Coutu, P., Shi, Y.F., Tardif, J.C., Nattel, S., St Arnaud, R., Dedhar, S., and Muller, W.J. (2006). Targeted ablation of ILK from the murine heart results in dilated cardiomyopathy and spontaneous heart failure. Genes Dev. *20*, 2355–2360. https://doi.org/10.1101/gad.1458906.

42. Bendig, G., Grimmler, M., Huttner, I.G., Wessels, G., Dahme, T., Just, S., Trano, N., Katus, H.A., Fishman, M.C., and Rottbauer, W. (2006). Integrin-linked kinase, a novel component of the cardiac mechanical stretch sensor, controls contractility in the zebrafish heart. Genes Dev. *20*, 2361–2372. https://doi.org/10.1101/gad.1448306.

43. Pracyk, J.B., Tanaka, K., Hegland, D.D., Kim, K.S., Sethi, R., Rovira, I.I., Blazina, D.R., Lee, L., Bruder, J.T., Kovesdi, I., et al. (1998). A requirement for the rac1 GTPase in the signal transduction pathway leading to cardiac myocyte hypertrophy. J. Clin. Invest. *102*, 929–937. https://doi.org/10.1172/JCI2552.

44. Hoshijima, M., Sah, V.P., Wang, Y., Chien, K.R., and Brown, J.H. (1998). The low molecular weight GTPase Rho regulates myofibril formation and organization in neonatal rat ventricular myocytes. Involvement of Rho kinase. J. Biol. Chem. *273*, 7725–7730.

45. Aikawa, R., Komuro, I., Yamazaki, T., Zou, Y., Kudoh, S., Zhu, W., Kadowaki, T., and Yazaki, Y. (1999). Rho family small G proteins play critical roles in mechanical stress-induced hypertrophic responses in cardiac myocytes. Circ. Res. *84*, 458–466.

46. Li, J., Liu, Y., Jin, Y., Wang, R., Wang, J., Lu, S., VanBuren, V., Dostal, D.E., Zhang, S.L., and Peng, X. (2017). Essential role of Cdc42 in cardiomyocyte proliferation and cell-cell adhesion during heart development. Dev. Biol. *421*, 271–283. https://doi.org/10.1016/j.ydbio.2016.12.012.

47. Brown, J.H., Del Re, D.P., and Sussman, M.A. (2006). The Rac and Rho hall of fame: a decade of hypertrophic signaling hits. Circ. Res. *98*, 730–742. https://doi.org/10.1161/01.RES.0000216039.75913.9e.

48. Schiller, H.B., Fernandez, I.E., Burgstaller, G., Schaab, C., Scheltema, R.A., Schwarzmayr, T., Strom, T.M., Eickelberg, O., and Mann, M. (2015). Time- and compartment-resolved proteome profiling of the extracellular niche in lung injury and repair. Mol. Syst. Biol. *11*, 819. https://doi.org/10.15252/msb.20156123.

49. Sharma, K., Schmitt, S., Bergner, C.G., Tyanova, S., Kannaiyan, N., Manrique-Hoyos, N., Kongi, K., Cantuti, L., Hanisch, U.K., Philips, M.A., et al. (2015). Cell type- and brain region-resolved mouse brain proteome. Nat. Neurosci. *18*, 1819–1831. https://doi.org/10.1038/nn.4160.

50. Hayashi, Y.K., Chou, F.L., Engvall, E., Ogawa, M., Matsuda, C., Hirabayashi, S., Yokochi, K., Ziober, B.L., Kramer, R.H., Kaufman, S.J., et al. (1998). Mutations in the integrin α7 gene cause congenital myopathy. Nat. Genet. *19*, 94–97. https://doi.org/10.1038/ng0598-94.

51. Mayer, U., Saher, G., Fässler, R., Bornemann, A., Echtermeyer, F., von der Mark, H., Miosge, N., Pöschl, E., and von der Mark, K. (1997). Absence of integrin α 7 causes a novel form of muscular dystrophy. Nat. Genet. *17*, 318–323. https://doi.org/10.1038/ng1197-318.

52. Bang, C., Batkai, S., Dangwal, S., Gupta, S.K., Foinquinos, A., Holzmann, A., Just, A., Remke, J., Zimmer, K., Zeug, A., et al. (2014). Cardiac fibroblast-derived microRNA passenger strand-enriched exosomes mediate cardiomyocyte hypertrophy. J. Clin. Invest. *124*, 2136–2146. https://doi.org/10.1172/JCI70577.

53. Hirt, M.N., Sörensen, N.A., Bartholdt, L.M., Boeddinghaus, J., Schaaf, S., Eder, A., Vollert, I., Stöhr, A., Schulze, T., Witten, A., et al. (2012). Increased afterload induces pathological cardiac hypertrophy: a new *in vitro* model. Basic Res. Cardiol. *107*, 307. https://doi.org/10.1007/s00395-012-0307-z.

54. Ridley, A.J. (2006). Rho GTPases and actin dynamics in membrane protrusions and vesicle trafficking. Trends Cell Biol. *16*, 522–529. https://doi.org/10.1016/j.tcb.2006.08.006.

55. Sussman, M.A., Welch, S., Walker, A., Klevitsky, R., Hewett, T.E., Price, R.L., Schaefer, E., and Yager, K. (2000). Altered focal adhesion regulation correlates with cardiomyopathy in mice expressing constitutively active rac1. J. Clin. Invest. *105*, 875–886. https://doi.org/10.1172/JCI8497.

56. Matsuda, C., Kameyama, K., Suzuki, A., Mishima, W., Yamaji, S., Okamoto, H., Nishino, I., and Hayashi, Y.K. (2008). Affixin activates Rac1 via βPIX in C2C12 myoblast. FEBS Lett. *582*, 1189–1196. https://doi.org/10.1016/j.febslet.2008.01.064.

57. Rosenberger, G., Jantke, I., Gal, A., and Kutsche, K. (2003). Interaction of αPIX (ARHGEF6) with β-parvin (PARVB) suggests an involvement of αPIX in integrin-mediated signaling. Hum. Mol. Genet. *12*, 155–167.

58. Onesto, C., Shutes, A., Picard, V., Schweighoffer, F., and Der, C.J. (2008). Characterization of EHT 1864, a novel small molecule inhibitor of Rac family small GTPases. Methods Enzymol *439*, 111–129. https://doi.org/10.1016/S0076-6879(07)00409-0.

59. de Jonge, H.W., Dekkers, D.H., Houtsmuller, A.B., Sharma, H.S., and Lamers, J.M. (2007). Differential signaling and hypertrophic responses in cyclically stretched vs endothelin-1 stimulated neonatal rat cardiomyocytes. Cell Biochem. Biophys. *47*, 21–32.

60. Yutao, X., Geru, W., Xiaojun, B., Tao, G., and Aiqun, M. (2006). Mechanical stretch-induced hypertrophy of neonatal rat ventricular myocytes is mediated by β(1)-integrin-microtubule signaling pathways. Eur. J. Heart Fail. *8*, 16–22. https://doi.org/10.1016/j.ejheart.2005.05.014.

61. Engler, A.J., Sen, S., Sweeney, H.L., and Discher, D.E. (2006). Matrix elasticity directs stem cell lineage specification. Cell *126*, 677–689. https://doi.org/10.1016/j.cell.2006.06.044.

62. Fung, Y.C. (1993). Biomechanics: Mechanical Properties of Living Tissues (Springer Verlag).

63. Chaturvedi, R.R., Herron, T., Simmons, R., Shore, D., Kumar, P., Sethia, B., Chua, F., Vassiliadis, E., and Kentish, J.C. (2010). Passive stiffness of myocardium from congenital heart disease and implications for diastole. Circulation *121*, 979–988. https://doi.org/10.1161/circulationaha.109.850677.

64. Fan, D., Takawale, A., Shen, M., Samokhvalov, V., Basu, R., Patel, V., Wang, X., Fernandez-Patron, C., Seubert, J.M., Oudit, G.Y., and Kassiri, Z. (2016). A disintegrin and metalloprotease-17 regulates pressure overload-induced myocardial hypertrophy and dysfunction through proteolytic processing of integrin β1. Hypertension *68*, 937–948. https://doi.org/10.1161/HYPERTENSIONAHA.116.07566.

65. Häuselmann, S.P., Rosc-Schlüter, B.I., Lorenz, V., Plaisance, I., Brink, M., Pfister, O., and Kuster, G.M. (2011). β1-Integrin is up-regulated via Rac1-dependent reactive oxygen species as part of the hypertrophic cardiomyocyte response. Free Radic. Biol. Med. *51*, 609–618. https://doi.org/10.1016/j.freeradbiomed.2011.05.007.

66. Schiller, H.B., Hermann, M.R., Polleux, J., Vignaud, T., Zanivan, S., Friedel, C.C., Sun, Z., Raducanu, A., Gottschalk, K.E., Théry, M., et al. (2013). β1- and αv-class integrins cooperate to regulate myosin II during rigidity sensing of fibronectin-based microenvironments. Nat. Cell Biol. *15*, 625–636. https://doi.org/10.1038/ncb2747.

67. Kong, F., Li, Z., Parks, W.M., Dumbauld, D.W., García, A.J., Mould, A.P., Humphries, M.J., and Zhu, C. (2013). Cyclic mechanical reinforcement of integrin-ligand interactions. Mol. Cell *49*, 1060–1068. https://doi.org/10.1016/j.molcel.2013.01.015.

68. Curtis, M., Nikolopoulos, S.N., and Turner, C.E. (2002). Actopaxin is phosphorylated during mitosis and is a substrate for cyclin B1/cdc2 kinase. Biochem. J. *363*, 233–242. https://doi.org/10.1042/0264-6021:3630233.

69. Clarke, D.M., Brown, M.C., LaLonde, D.P., and Turner, C.E. (2004). Phosphorylation of actopaxin regulates cell spreading and migration. J. Cell Biol. *166*, 901–912. https://doi.org/10.1083/jcb.200404024.

70. LaLonde, D.P., Brown, M.C., Bouverat, B.P., and Turner, C.E. (2005). Actopaxin interacts with TESK1 to regulate cell spreading on fibronectin. J. Biol. Chem. *280*, 21680–21688. https://doi.org/10.1074/jbc.M500752200.

71. Mishima, W., Suzuki, A., Yamaji, S., Yoshimi, R., Ueda, A., Kaneko, T., Tanaka, J., Miwa, Y., Ohno, S., and Ishigatsubo, Y. (2004). The first CH domain of affixin activates Cdc42 and Rac1 through alphaPIX, a Cdc42/Rac1-specific guanine nucleotide exchanging factor. Genes Cells *9*, 193–204. https://doi.org/10.1111/j.1356-9597.2004.00717.x.

72. Sopko, N., Qin, Y., Finan, A., Dadabayev, A., Chigurupati, S., Qin, J., Penn, M.S., and Gupta, S. (2011). Significance of thymosin β4 and implication of PINCH-1-ILK-α-parvin (PIP) complex in human dilated cardiomyopathy. PLoS One *6*, e20184. https://doi.org/10.1371/journal.pone.0020184.

73. Chu, H., Thievessen, I., Sixt, M., Lämmermann, T., Waisman, A., Braun, A., Noegel, A.A., and Fässler, R. (2006). γ-Parvin is dispensable for hematopoiesis, leukocyte trafficking, and T-cell-dependent antibody response. Mol. Cell. Biol. *26*, 1817–1825. https://doi.org/10.1128/mcb.26.5.1817-1825.2006.

74. Cox, J., Neuhauser, N., Michalski, A., Scheltema, R.A., Olsen, J.V., and Mann, M. (2011). Andromeda: a peptide search engine integrated into the MaxQuant environment. J. Proteome Res. *10*, 1794–1805. https://doi.org/10.1021/pr101065j.

75. Tyanova, S., Temu, T., Sinitcyn, P., Carlson, A., Hein, M.Y., Geiger, T., Mann, M., and Cox, J. (2016). The Perseus computational platform for comprehensive analysis of (prote)omics data. Nat. Methods *13*, 731–740. https://doi.org/10.1038/nmeth.3901.

76. Kah, D., Winterl, A., Přechová, M., Schöler, U., Schneider, W., Friedrich, O., Gregor, M., and Fabry, B. (2021). A low-cost uniaxial cell stretcher for six parallel wells. HardwareX *9*, e00162. https://doi.org/10.1016/j.ohx.2020.e00162.

77. Lautscham, L.A., Kämmerer, C., Lange, J.R., Kolb, T., Mark, C., Schilling, A., Strissel, P.L., Strick, R., Gluth, C., Rowat, A.C., et al. (2015). Migration in confined 3D environments is determined by a combination of adhesiveness, nuclear volume, contractility, and cell stiffness. Biophys. J. *109*, 900–913. https://doi.org/10.1016/j.bpj.2015.07.025.

78. Nolte, H., Hölper, S., Selbach, M., Braun, T., and Krüger, M. (2014). Assessment of serum protein dynamics by native SILAC flooding (SILflood). Anal. Chem. *86*, 11033–11037. https://doi.org/10.1021/ac502883p.

79. Böttcher, R.T., Veelders, M., Rombaut, P., Faix, J., Theodosiou, M., Stradal, T.E., Rottner, K., Zent, R., Herzog, F., and Fässler, R. (2017). Kindlin-2 recruits paxillin and Arp2/3 to promote membrane protrusions during initial cell spreading. J. Cell Biol. *216*, 3785–3798. https://doi.org/10.1083/jcb.201701176.

80. Auernheimer, V., Lautscham, L.A., Leidenberger, M., Friedrich, O., Kappes, B., Fabry, B., and Goldmann, W.H. (2015). Vinculin phosphorylation at residues Y100 and Y1065 is required for cellular force transmission. J. Cell Sci. *128*, 3435–3443. https://doi.org/10.1242/jcs.172031.

81. Thievessen, I., Fakhri, N., Steinwachs, J., Kraus, V., McIsaac, R.S., Gao, L., Chen, B.C., Baird, M.A., Davidson, M.W., Betzig, E., et al. (2015). Vinculin is required for cell polarization, migration, and extracellular matrix remodeling in 3D collagen. FASEB J. *29*, 4555–4567. https://doi.org/10.1096/fj.14-268235.

82. Sakai, T., Li, S., Docheva, D., Grashoff, C., Sakai, K., Kostka, G., Braun, A., Pfeifer, A., Yurchenco, P.D., and Fässler, R. (2003). Integrin-linked kinase (ILK) is required for polarizing the epiblast, cell adhesion, and controlling

actin accumulation. Genes Dev. *17*, 926–940. https://doi.org/10.1101/gad.255603.

83. Yamaji, S., Suzuki, A., Sugiyama, Y., Koide, Y., Yoshida, M., Kanamori, H., Mohri, H., Ohno, S., and Ishigatsubo, Y. (2001). A novel integrin-linked kinase-binding protein, affixin, is involved in the early stage of cell-substrate interaction. J. Cell Biol. *153*, 1251–1264.
84. Fässler, R., and Meyer, M. (1995). Consequences of lack of β 1 integrin gene expression in mice. Genes Dev. *9*, 1896–1908.
85. Zhang, D., Gaussin, V., Taffet, G.E., Belaguli, N.S., Yamada, M., Schwartz, R.J., Michael, L.H., Overbeek, P.A., and Schneider, M.D. (2000). TAK1 is activated in the myocardium after pressure overload and is sufficient to provoke heart failure in transgenic mice. Nat. Med. *6*, 556–563. https://doi.org/10.1038/75037.
86. Tiemann, K., Weyer, D., Djoufack, P.C., Ghanem, A., Lewalter, T., Dreiner, U., Meyer, R., Grohe, C., and Fink, K.B. (2003). Increasing myocardial contraction and blood pressure in C57BL/6 mice during early postnatal development. Am. J. Physiol. Heart Circ. Physiol. *284*, H464–H474. https://doi.org/10.1152/ajpheart.00540.2002.
87. Moser, M., Imhof, A., Pscherer, A., Bauer, R., Amselgruber, W., Sinowatz, F., Hofstädter, F., Schüle, R., and Buettner, R. (1995). Cloning and characterization of a second AP-2 transcription factor: AP-2 β. Development *121*, 2779–2788.

Please cite this article in press as: Thievessen et al., The focal adhesion protein β-parvin controls cardiomyocyte shape and sarcomere assembly in response to mechanical load, Current Biology (2022), https://doi.org/10.1016/j.cub.2022.05.047

STAR★METHODS

KEY RESOURCES TABLE

REAGENT or RESOURCE	SOURCE	IDENTIFIER
Antibodies		
Mouse monoclonal anti ILK	BD Bioscience	Cat#611803; RRID: AB_399283
Mouse monoclonal anti Caveolin3	BD Bioscience	Cat#610421; RRID: AB_397801
Mouse monoclonal anti Rac1	BD Bioscience	Cat#610651; RRID: AB_397978
Mouse monoclonal anti GAPDH	Sigma-Aldrich	Cat#G8795; RRID: AB_1078991
Rat monoclonal anti Integrin beta1	Millipore	Cat# MAB1997; RRID: AB_2128202
Rabbit polyclonal anti α-parvin	Chu et al.[73]	N/A
Rabbit polyclonal anti β-parvin	Chu et al.[73]	N/A
Rabbit polyclonal anti γ-parvin	Chu et al.[73]	N/A
Mouse monoclonal anti alpha-Actinin	Sigma-Aldrich	Cat# A7811; RRID: AB_476766
Anti-GFP	BD Bioscience/Clontech	Cat# 8367-2
Anti-GST Antibody, HRP Conjugated	GE Healthcare	Cat# RPN1236; RRID: AB_771429
Mouse monoclonal anti Sarcomeric Alpha Actinin	Abcam	Cat# ab9465; RRID: AB_307264
Goat polyclonal anti Cardiac Troponin I	Abcam	Cat# ab56357; RRID: AB_880622
Mouse monoclonal anti Vinculin	Sigma-Aldrich	Cat# V4505; RRID: AB_477617
Rabbit polyclonal anti AKT	Cell Signaling Technology	Cat# 9272; RRID: AB_329827
Rabbit polyclonal anti Phospho-Akt (Ser473)	Cell Signaling Technology	Cat# 9271; RRID: AB_329825
Phalloidin-TRITC	Sigma-Aldrich	Cat# P1951; RRID: AB_2315148
Goat anti Mouse IgG (H L)-HRP Conjugate	Bio-Rad	Cat# 170-6516; RRID: AB_11125547
Goat anti Rabbit IgG (H L)-HRP Conjugate	Bio-Rad	Cat# 170-6515; RRID: AB_11125142
Fluorescein (FITC)-AffiniPure Donkey Anti-Mouse IgG (H+L)	Jackson ImmunoResearch Labs	Cat# 715-095-151; RRID: AB_2335588
Rhodamine (TRITC)-AffiniPure Donkey Anti-Mouse IgG (H+L)	Jackson ImmunoResearch Labs	Cat# 715-025-150; RRID: AB_2340766
Cy2-AffiniPure Donkey Anti-Rabbit IgG (H+L)	Jackson ImmunoResearch Labs	Cat# 711-225-152; RRID: AB_2340612
Rhodamine (TRITC)-AffiniPure Donkey Anti-Rabbit IgG (H+L)	Jackson ImmunoResearch Labs	Cat# 711-025-152; RRID: AB_2340588
Rhodamine (TRITC)-AffiniPure Donkey Anti-Rat IgG (H+L)	Jackson ImmunoResearch Labs	Cat# 712-025-150; RRID: AB_2340635
Bacterial and virus strains		
E.coli XL1-Blue competent cells	Agilent	Cat# 200249
Biological samples		
P3 rat cardiomyocytes	This paper	N/A
P1-2 mouse cardiomyocytes	This paper	N/A
Parvb genomic DNA	Human Genome Mapping Project Center, Cambridge	PAC-clone #597-O14
Chemicals, peptides, and recombinant proteins		
Fibronectin	Roche	Cat# 11080938001
4',6-diamidino-2-phenylindole (DAPI)	Carl Roth	Cat# 6335.1
Hoechst 33342	Sigma-Aldrich	Cat# 62249
Ibidi Mounting medium	Ibidi	Cat# 50001
Collagen Type I, rat tail collagen R	Matrix Bioscience	Cat# 50301
Collagen Type I, bovine skin collagen G	Matrix Bioscience	Cat# 50104
DMEM-F12/Glutamax TM-1	Thermo Fischer Scientific	Cat# 10565018
Dulbecco's Modified Eagle Medium (DMEM), high glucose, GlutaMAX	Thermo Fisher Scientific	Cat# 61965059
Ara-C	Sigma-Aldrich	Cat# C1768
Opti-MEM I Reduced Serum Medium	Thermo Fisher Scientific	Cat# 11058021
DRAQ5	Thermo Fisher Scientific	Cat# 62251

(*Continued on next page*)

Please cite this article in press as: Thievessen et al., The focal adhesion protein β-parvin controls cardiomyocyte shape and sarcomere assembly in response to mechanical load, Current Biology (2022), https://doi.org/10.1016/j.cub.2022.05.047

Continued

REAGENT or RESOURCE	SOURCE	IDENTIFIER
Horse Serum	Thermo Fisher Scientific	Cat# 16050122
Fetal Bovine Serum (FBS)	biowest	Cat# S1810
Penicillin-Streptomycin	Thermo Fisher Scientific	Cat# 15140122
Insulin-Transferrin-Selenium-Sodium Pyruvate (ITS-A) (100X)	Thermo Fisher Scientific	Cat# 51300044
IGF-1, human recombinant	Thermo Fisher Scientific	Cat# PHG0071
Phenylephrine	Sigma-Aldrich	Cat# P6126
Rac1-inhibitor EHT1864	Cayman Chemical Company	Cat# 17258
DPBS, no calcium, no magnesium	Thermo Fisher Scientific	Cat# 14190094
Lipofectamine RNAiMAX	Thermo Fisher Scientific	Cat# 13778150
Lipofectamine LTX	Thermo Fisher Scientific	Cat# 15338100
GlycoBlue Coprecipitant	Thermo Fisher Scientific	Cat# AM9516
Acrylamide-Bisacrylamide solution, 29:1	Sigma-Aldrich	Cat# A7802
Sulfo-SANPAH	Thermo-Fisher	Cat# 22589
Trichlor-(1H,1H,2H,2H-perfluoroctyl)-silan	Sigma-Aldrich	Cat# 448931
Paraplast X-tra	Sigma-Aldrich	Cat# P3808
TRIzol Reagent	Thermo Fisher	Cat# 15596026
^{33}P-UTP	Amersham	N/A
^{32}P-dCTP	Amersham	N/A
Protease-inhibitor cocktail Complete Mini	Roche	Cat# 11836153001
Phosphatase-inhibitor cocktail	Roche	Cat# 4906837001
Streptavidin-Sepharose beads	Amersham	Cat# 17-5113-01
Critical commercial assays		
Neonatal Heart Disassociation Kit	Miltenyi Biotec	Cat# 130-098-373
M-MLV Reverse Transcriptase	Sigma	Cat# M1302
Pierce 660nm protein assay	Thermo Fisher	Cat# 22660
NEBuilder Hifi DNA Assembly Kit	New England Biolabs	Cat# E2621L
Cold Fusion Cloning Kit with Competent Cells	System Biosciences	Cat# MC010B-1
In Fusion HD Cloning Kit	Clontech	Cat# 638909
ViraPower Adenoviral Expression System	Invitrogen	Cat# K4930-00
RNeasy Kit	Qiagen	Cat# 74106
Sylgaard 184 Silicone Elastomer Kit	Dow Chemical Company/VWR	Cat# 634165S
RedTaq Mastermix 2-fold DNA-Polymerase	Genaxxon	Cat# M3029
RediPrime II random prime labeling	Amersham	N/A
Deposited data		
Cardiac proteomics data	This paper	Proteome Xchange Consortium; PRIDE: PXD033963
Experimental models: Cell lines		
Human: HEK293	ATCC	Cat# PTA-4488; RRID: CVCL_0045
R1 murine ES-cells	ATCC	Cat# SCRC-1011; RRID: CVCL_2167
Experimental models: Organisms/strains		
Sprague Dawley Rats	Charles River	RRID: RGD_737891
Parvb$^{-/-}$-mice (mixed background 129/sv/C57Bl/6J)	This paper	N/A
Oligonucleotides		
Negative control-siRNA, Silencer Select	Thermo Fisher	ID: #4390843
Parvb-siRNA, Silcencer Select pre-designed	Thermo Fisher	ID: #s170128
Parvb-siRNA, Flexitube	Qiagen	#SI01828519
Parvb I2 forward primer, genotypg. GTG AAC TTC ACT GGA CTC TT	This paper	N/A

(*Continued on next page*)

Please cite this article in press as: Thievessen et al., The focal adhesion protein β-parvin controls cardiomyocyte shape and sarcomere assembly in response to mechanical load, Current Biology (2022), https://doi.org/10.1016/j.cub.2022.05.047

Continued

REAGENT or RESOURCE	SOURCE	IDENTIFIER
PGK forward primer (neomycin cassette), genotypg. GAT TAG ATA AAT GCC TGC TC	This paper	N/A
Parvb E3 reverse primer, genotypg. TCC TTG AAC TTG GGG TCT TCT	This paper	N/A
Parvb forward primer, RT-PCR GACTGGATCAACGACGTGC	This paper	N/A
Parvb reverse primer, RT-PCR TGCACGGTGACGTGTTCAGG	This paper	N/A
GAPDH forward primer, RT-PCR CAG AAG ACT GTG GAT GGC CC	This paper	N/A
GAPDH reverse primer, RT-PCR AGT GTA GCC CAG GAT GCC CT	This paper	N/A
Recombinant DNA		
pEGFP-C1	Clontech	Cat# 6084-1
pEGFP-α-parvin	This paper	N/A
pEGFP-β-parvin	This paper	N/A
pEGFP-α-skeletal muscle tropomyosin	David Helfman	N/A
pEGFP-Rac1-Q61L	This paper	N/A
pEGFP-Rac1-T17N	This paper	N/A
pRRLSIN.cPPT.PGK-GFP.WPRE	Didier Trono	Addgene, RRID: 12252
pLentiGFP	This paper	N/A
pLentiGFP-α-parvin	This paper	N/A
pLentiGFP-β-parvin	This paper	N/A
pENTR1A	Thermo Fisher	Cat# A10462
pAdCMV/V5/DEST	Invitrogen	V49320
pAdGFP	This paper	N/A
pAdGFP-α-parvin	This paper	N/A
pAdGFP-β-parvin	This paper	N/A
Software and algorithms		
Leica LAS AF Image Acquisition Software	Leica Microsystems	N/A
ZEN Blue	Carl Zeiss AG	RRID: SCR_013672
Fiji	http://fiji.sc	RRID: SCR_002285
GraphPad Prism	GraphPad Prism	RRID: SCR_002798
MaxQuant	Cox et al.[74]	RRID: SCR_014485
Perseus	Tyanova et al.[75]	RRID: SCR_015753
Other		
Leica SP5X upright confocal microscope system	Leica Microsystems	N/A
Zeiss LSM800 confocal laser scanning microscope with Airyscan module	Carl Zeiss AG	N/A
Leica DMI 6000 epifluorescence microscope system	Leica Microsystems	N/A
Axioskop transmitted light microscope	Carl Zeiss AG	N/A
Axio Imager Z1 epifluorescence microscope	Carl Zeiss AG	N/A
MZFLIII Binocular	Leica Microsystems	N/A
Custom made uni-axial cell stretcher device	Kah et al.[76]	N/A
Spinning disk device	Lautscham et al.[77]	N/A
GentleMACS Octo Dissociator	Milteny Biotech	N/A
Ultra-high performance liquid chromatography, Easy nLC1000	Thermo Fisher Scientific	N/A
QExactive mass spectrometer	Thermo Fisher Scientific	N/A
Exer3/6 treadmill	Columbus Instruments, USA	N/A

(*Continued on next page*)

Please cite this article in press as: Thievessen et al., The focal adhesion protein β-parvin controls cardiomyocyte shape and sarcomere assembly in response to mechanical load, Current Biology (2022), https://doi.org/10.1016/j.cub.2022.05.047

Continued

REAGENT or RESOURCE	SOURCE	IDENTIFIER
HDI-5000 ultrasound system, echocardiography	Philips Medical Systems, USA	N/A
Ultramicrotome	Reichert	N/A
Transmission electron microscope 902A	Carl Zeiss AG	N/A
HM 355 S Mikrotom	Mikrom	N/A
HM 500 OM Mikrotom	Mikrom	N/A
Hybond N+ Nylon membrane	Amersham	N/A
PVDF-membrane	Carl Roth	T830.1
Lung proteomics data	Schiller et al.[48]	ProteomeXchange Consortium/ PRIDE partner repository #PXD001765
Brain proteomics data	Sharma et al.[49]	ProteomeXchange Consortium/ PRIDE partner repository #PXD001250

RESOURCE AVAILABILITY

Lead contact

Further information and requests for resources and reagents should be directed to and will be fulfilled by the lead contact, Reinhard Fässler (faessler@biochem.mpg.de)

Materials availability

All unique/stable reagents generated in this study are available from the lead contact without restriction.

Data and code availability

- Cardiac proteomics data have been deposited at PRIDE and are publicly available as of date of publication. The accession number is listed in the key resources table.
- All data reported in this study will be shared by the lead contact upon request.
- This paper does not report any original code.
- Any additional information required to reanalyze the data reported in this paper is available from the lead contact upon request.

EXPERIMENTAL MODEL AND SUBJECT DETAILS

Animals

Sprague-Dawley rats were obtained from Charles River Laboratories (Cologne, Germany) or bred in house at the animal facility of the Friedrich-Alexander-University of Erlangen-Nuremberg. Parvb$^{-/-}$-mice were generated using R1-embryonic stem cells (sv/129-strain) and blastocysts derived from C57Bl/6J-mice. Parvb$^{+/-}$-mice were kept on the mixed genetic background (sv/129/C57Bl/6J). Control and Parvb$^{-/-}$-littermates of 2-6 months age were used for experiments.

Housing and use of laboratory animals at the Max Planck Institute of Biochemistry, the Friedrich-Alexander-University and the German Sports University fully conform with all German (e.g. German Animal Welfare Act) and EU (e.g. Annex III of Directive 2010/63/EU of the European Parliament on the protection of animals used for scientific purposes) applicable laws and regulations concerning care and use of laboratory animals, and have been approved by the District Government of Upper Bavaria (No.5.1-568 rural districts office), the Animal Ethics Committee of the Friedrich-Alexander University of Erlangen-Nuremberg (heart dissection from neonatal mice and rats: protocol TS-7/2015 Biophysik (NMVC), protocol TS-9/2016 Nephropatho (NRVC)), and the Animal Care Committee of Northrine-Westfalia (transverse aortic constriction and treadmilling exercise), respectively. Animals were housed in environmentally controlled animal facilities, usually in sex-matched groups or in stable breeder pairs or trios, at a 12:12h light:dark cycle, and with food and water available ad libitum.

Isolation and culture of NRVC/NMVC

NRVC

Dissected hearts from neonatal (postnatal day 3; P3) Sprague-Dawley rats were isolated using the Neonatal Heart Dissociation Kit (Miltenyi Biotec, Bergisch Gladbach, Germany) and the Octo Dissociator (Miltenyi Biotec, Bergisch Gladbach, Germany) according to manufacturer's instructions. For P3 cardiomyocyte enrichment, cells were preplated for 1.5 h in DMEM-F12/Glutamax TM-I (Life Technologies, Darmstadt, Germany)/10% fetal bovine serum (FBS, Biowest, Nuaille, France)/penicillin (100 U/ml)/streptomycin (100 mg/ml) (Life Technologies), non-attached cells collected, centrifuged for 5 min at 330 x g, resuspended and cultured at

Please cite this article in press as: Thievessen et al., The focal adhesion protein β-parvin controls cardiomyocyte shape and sarcomere assembly in response to mechanical load, Current Biology (2022), https://doi.org/10.1016/j.cub.2022.05.047

50-60% confluency in cardiomyocyte medium (DMEM-F12/Glutamax TM-I (Thermo Fisher Scientific)/5% fetal bovine serum (FBS, Biowest, Nuaille, France)/5% Horse serum (Thermo Fisher Scientific)/3 mM Na-pyruvate/insulin/transferrin-selenite (1:100, Thermo Fischer)/0.2% BSA/penicillin (100 U/ml)/streptomycin (100 mg/ml)/20 μM Ara-C (Sigma-Aldrich)) on collagen I coated (50 μg/ml, Matrix Bioscience) cover slips, cell culture vessels or Poly-dimethylsiloxane (PDMS)-based flexible membranes, or used to generate 3D cardiac microtissues.

NMVC

Dissected hearts from neonatal (P1-2) control and Parvb$^{-/-}$ mice (2-3 animals/group) were minced with a scissor and dissociated using the Neonatal Heart Dissociation kit (Miltenyi Biotec, Bergisch Gladbach, Germany) in 0.45 ml enzyme mix/heart in a 2 ml reaction tube for 1 h at 37°C under constant end-to-end rotation and gentle pipetting every 10-15 min, passed through a 100 μm cell strainer and centrifuged at 330 x g for 5 min. The pellet was resuspended in 1 ml cardiomyocyte medium (DMEM-F12/Glutamax TM-1(Life technologies) containing 5% horse serum, 5% FCS, 20μM ara-C, 3mM Na-pyruvate, 0.1mM ascorbic acid, insulin/transferrin-selenite, 0.2% BSA and 100U/ml penicillin streptomycin)/heart and pre-plated onto non-coated cell culture dishes for 90 min to remove cardiac fibroblasts. The supernatant was distributed in two wells of a 24-well plate/heart, each containing a collagen I coated (50 μg/ml; Matrix Bioscience #50301) 12 mm round coverslip, and cultured for up to 4 days before fixation and immunofluorescence staining. The morphological analyses of control and Parvb$^{-/-}$ NMVCs were performed in three biological replicates.

HEK293T cells

HEK293 cells were purchased from ATCC and are from female origin. The cells were cultured in monolayers in DMEM/Glutamax (Thermo Fischer) supplemented with 10% FBS (Thermo Fisher Scientific) and antibiotics at 37°C in a 5% CO2 incubator.

METHOD DETAILS

Heart proteome analysis

Dissected hearts of adult mice were snap frozen in liquid nitrogen, ground to a fine powder using a mortar and pestle and proteins extracted with RIPA lysis buffer (100 mM Tris/HCl, pH 7.5, 300 mM NaCl, 2 mM EDTA, 2% NP40, 0.2% Na-deoxycholate). Lysates were homogenized using a Bioruptor, sheared with a G17 needle and clarified by centrifugation. Protein concentrations were determined using the Pierce 660nm protein assay (Thermo Fisher Scientific). 20 μg lysate were precipitated with acetone in the presence of GlycoBlue (Thermo Fisher Scientific) for 2 h at −20°C, washed with 90% acetone and resuspended in Bolt LDS sample buffer (Invitrogen). Proteins were reduced with 20 mM DTT for 30 min at RT, carbamidomethylated with 10 mM iodoacetamide for 20 min in the dark at RT and subsequently separated using a Bolt 4-12% Bis-Tris Plus gel (Invitrogen). After Coomassie-staining, each sample was cut into seven equal-sized slices, destained with 50% acetonitrile (ACN) and dehydrated with 100% ACN. Proteins were digested overnight at 37°C with Lys-C and trypsin (12 ng/μl, 1:10) and on the following day digestion was stopped by adding trifluoroacetic acid. Tryptic peptides were extracted using increasing concentrations of ACN. Organic compounds were evaporated using a SpeedVac concentrator (Eppendorf) and peptides were loaded onto conditioned C18 cartridges and washed with 20 μl of 0.1% TFA.

Proteomic analysis was performed using an Easy nLC 1000 ultra-high performance liquid chromatography (UHPLC) coupled to a QExactive mass spectrometer (Thermo Fisher Scientific) with the previously described settings.[78] The raw files were processed using MaxQuant software and its implemented Andromeda search engine.[74] The experiment was performed once. Statistical analysis, and t tests were performed using Perseus software.[75] The mass spectrometry proteomics data have been deposited to the ProteomeXchange Consortium via the PRIDE partner repository with the dataset identifier PRIDE: PXD033963.

siRNA-mediated knockdown of Parvb in NRVCs

NRVCs on 2D surfaces were transfected 24 h after isolation/seeding. NRVCs for 3D cardiac microtissues were transfected in suspension immediately after cell isolation for 30 minutes. The cell-containing lipofection-mix was subsequently added to the collagen-solution used for the top-layer preparation of the microtissues (see below).

NRVCs were transfected with different *Parvb*-specific and non-specific control siRNA (Thermo Fisher Silencer Select pre-designed siRNA ID #s170128 and Silencer Select negative control siRNA #4390843 (10 pmol/1.2x10^5 cells); Qiagen Flexitube siRNA #SI01828519 (20 pmol/1.2x10^5 cells)) using RNAiMax transfection reagent (Thermo Fisher Scientific) according to manufacturer's instructions. 48 h after siRNA transfection, mRNA was isolated using RNeasy kit (Qiagen, Hilden, Germany) according to manufacturer's instructions, and subjected to RT-PCR analysis using *Parvb*- and *GAPDH*-specific primers (ParvbF 5′-GACTGGATCAAC GACGTGC-3′, ParvbR 5′-TGCACGGTGACGTGTTCAGG-3′; GAPDHF 5′- CAGAAGACTGTGGATGGCCC-3′ and GAPDHR 5′-AGTGTAGCCCAGGATGCCCT-3′) to confirm successful *Parvb*-mRNA depletion. The Life Technologies Silencer Select system was consistently used throughout further experiments.

Viral expression of murine α- and β-parvin in NRVCs

For lentiviral expression of β-parvin, EGFP-tagged murine β-parvin or EGFP alone was subcloned into the lentiviral vector pRRLSIN.cPPT.PGK-GFP.WPRE by in-fusion cloning (Clontech). pRRLSIN.cPPT.PGK-GFP.WPRE was from Addgene (plasmid # 12252; http://n2t.net/addgene:12252; RRID:Addgene_12252). Vesicular stomatitis virus G pseudotyped lentiviruses were produced by transient transfection of 293T cells as described previously.[79] Cells were transfected using Lipofectamine 2000 according to the

Please cite this article in press as: Thievessen et al., The focal adhesion protein β-parvin controls cardiomyocyte shape and sarcomere assembly in response to mechanical load, Current Biology (2022), https://doi.org/10.1016/j.cub.2022.05.047

manufacturer's protocol, viral particles were harvested after 48-72 h by collecting the cell culture medium, followed by filtration (0.45 μm) and ultracentrifugation at 20,300 rpm for 2 h in a SW 32 Ti rotor (Beckman Coulter) and resuspension in 45 μl Hank's balanced salt solution (Thermo Fisher Scientific). To rescue the loss of β-parvin in *Parvb*-siRNA NRVC, the cells were infected with either EGFP-β-parvin- or EGFP-expressing lentivirus 24 h after *Parvb*-siRNA transfection and fixed for analysis 48 h later. Lentiviral rescue was performed in three biological replicates.

For adenoviral expression of α- and β-parvin, EGFP-tagged α- or β-parvin, or EGFP alone was subcloned into the pENTR1A by DNA assembly (NEBuilder Hifi DNA Assembly Kit) and transferred by Gateway recombinase into the adenoviral expression plasmid pAdCMV/V5/DEST (Invitrogen). After adenovirus production in 293T cells (ViraPower Adenoviral Expression System; Thermo Fisher Scientific), control- and *Parvb*-siRNA-treated NRVCs were transduced with either EGFP-α-, or EGFP-β-parvin- or EGFP-only-expressing adenovirus, fixed with 4% PFA 48 h later and analyzed. Experiments were performed in biological triplicates.

Transient expression of skeletal muscle tropomyosin-GFP and GFP-Rac1-Q61L/T17N in NRVCs

cDNAs of human Rac1-Q61L and -T17N, and α-skeletal muscle tropomyosin, subcloned into the pEGFP-C1 backbone were transfected into NRVCs using Lipofectamine LTX according to the manufacturer's instructions. 24 h later, cells were either live imaged (skTM-GFP) or fixed and immunostained (GFP-Rac1-Q61L/T17N).

NRVC culture on flexible polyacrylamide substrates

Flexible polyacrylamide (PAA) substrates were prepared as described previously.[80] Briefly, acrylamide-bisacrylamide gels (29:1; Sigma-Aldrich) of 5.8 % (10 kPa) and 8.0 % (50 kPa) were cast on glutaraldehyde-activated coverslips, subsequently covered with 0.5 mg/ml Sulfo-SANPAH (Thermo Fisher Scientific) and activated for 5 min under UV-light, washed 2x 10 min with PBS, and coated with collagen I (100 μg/ml; Matrix Bioscience #50301) at 4°C overnight. The substrates were washed once with PBS. NRVCs were seeded onto the substrates at 50-60% confluency and allowed to adhere and spread over night before siRNA-lipofection, followed by fixation, immunofluorescence staining and confocal imaging.

Uni-axial stretching of NRVCs on 2D PDMS membranes

Poly-dimethylsiloxane (PDMS) based 2D membrane devices were generated by casting de-gassed PDMS (Dow Corning Sylgaard 184) at a mixing ratio of 32:1 (elastomer:curing agent) in plastic molds. Casts were baked for 24 h at 65°C and removed from molds under isopropanol, cleaned with isopropanol and air-dried under sterile conditions. 250 μl Sulfo-SANPAH (0.5 mg/ml; Thermo Fisher Scientific) was added onto the gel prior to UV-light exposure for 5 min, followed by 2x 10 min washing (PBS) and incubation with 100 μg/ml collagen I solution (Matrix Bioscience #50301) at 4°C over night. Each membrane device was mounted into a rack fitting into a custom build, stepper-motor driven and PC-controlled, uni-axial stretcher device and washed once with PBS before cell seeding. Freshly isolated NRVCs were seeded onto the membranes at a confluency of 50-60% and allowed to adhere and spread over night before siRNA-lipofection and subsequent application of uni-axial stretch (8%, 1 Hz, 48 h) to the membranes, followed by fixation, immunofluorescence staining and confocal imaging in the racks.

Spinning disk adhesion assay

NRVCs were cultured on collagen I coated (50 μg/ml Matrix Bioscience #50301) cell culture dishes and stained with Hoechst 33342 (Sigma-Aldrich) immediately prior to the assay. Cell adhesion was quantified using a customized microscope stage mounted device consisting of a compressed air driven, rotating glass plate as described previously.[77] The glass plate was located 100 μm above the culture dish and rotated at 1750 rpm for 400 s to apply shear force. Regions at the same radial distance from the center in control- and *Parvb*-siRNA treated samples were imaged before and after the spin. The fraction of adherent cells was calculated after superimposing pre- and post-spin images as the ratio of pre-spin/pre+post-spin labeled nuclei.

Generation of 3D cardiac microtissues and quantification of forces

PDMS-based 3D microtissue devices, carrying an array of 6x3 cuboid shaped wells (4x2x2 mm), each containing two microposts of 500 μm diameter and 2 mm height were generated by casting de-gassed PDMS (Dow Chemical Sylgard 184) at a mixing ratio of 22:1 (elastomer:curing agent) in Computerized Numerical Control- (CNC) machined, Trichlor-(1H,1H,2H,2H-perfluoroctyl)-silan (Sigma-Aldrich) coated steel molds. Casts were baked for 24 h at 65°C and removed from molds under isopropanol. Microtissue devices were cleaned with isopropanol and air-dried under sterile conditions. Collagen I solution (0.3 mg/ml) was prepared as previously described.[81] In brief, a 0.3 mg/ml collagen I solution containing 0.1 mg/ml collagen R (rat tail collagen I; Matrix Bioscience #50301), 0.2 mg/ml collagen G (bovine skin collagen I; Matrix Bioscience #50104), and 25 mM $NaHCO_3$ in DMEM was prepared under sterile conditions on ice. Collagen polymerization was induced by adjusting the pH to ~10 through the addition of NaOH to a final concentration of 15 mM. The wells were filled up to 50% of the total well volume (6 μl) as a non-cell containing collagen bottom layer to prevent cell sinking to the bottom of the well during polymerization of the cell containing top layer. Pipetting was performed on ice and the devices were incubated for 2 h at 37°C, 95% humidity and 5% CO_2 for bottom layer polymerization. Subsequently, the cell containing collagen top layer was pipetted onto the bottom layer using collagen I solution identical to the bottom layer solution mixed with freshly isolated NRVCs ($2x10^5$ cells per well/microtissue), allowing NRVCs to sink on top of the pre-polymerized bottom layer. Microtissue preparations were incubated for 15 h at 37°C, 95% humidity and 5% CO_2 before adding cardiomyocyte medium.

Please cite this article in press as: Thievessen et al., The focal adhesion protein β-parvin controls cardiomyocyte shape and sarcomere assembly in response to mechanical load, Current Biology (2022), https://doi.org/10.1016/j.cub.2022.05.047

Contractile forces generated by cardiac microtissues were calculated based on the microtissue-induced deflection of microposts. Bright field time lapse image sequences (25 ms frame rate) of spontaneously contracting microtissues were recorded at 37°C using a Leica DMI 6000-based inverted transmitted light microscope system and a 5X/0.12NA objective lens. Micropost deflection was recorded at the post tips and interpolated to the microtissue position along the post length (i.e. tissue height measured from the bottom of the well). Contractile forces were calculated from maximum post deflections based on Hooke's Law. The spring constant of the microposts was 1 μN for a lateral deflection of 1 μm at a typical tissue height of 1.25 mm.

Microscopy and morphological analysis of NRVCs/NMVCs

Confocal imaging of NRVCs and NMVCs on mounted coverslips and PDMS-membranes was performed on an upright SP5X laser scanning confocal microscope (Leica, Wetzlar, Germany) using a 20X/1.0NA dip-in water-immersion objective lens. 3D image stacks of 370 x 370 μm were recorded at 1 μm z-section distance throughout the thickness of the sample. Confocal image stacks were maximum-projected prior to morphological analysis. Cells were outlined manually (ImageJ; National Institutes of Health, Bethesda, Maryland, USA) to determine cell area, cell perimeter, major axis and minor axis length, and aspect ratio. Minimum outer bounding ellipses to quantify the extension range of SCPs were manually fitted to cells using ImageJ software. High resolution imaging of sarcomere organization and focal adhesions in fixed cells was performed on an upright Zeiss LSM 800 microscope system (Zeiss, Jena, Germany) using a 63X/1.4NA Plan Apo objective lens. 3D image stacks of 67 x 67 μm were recorded at 0.4 μm z-section distance throughout the thickness of the sample. Maximum-projected image stacks (sarcomere organization) or individual z-sections (focal adhesions) are shown. Maximum projected images for the analysis of Z-disk morphology were equally thresholded between control- and *Parvb*-siRNA groups and analyzed for Z-disk width and aspect ratio (ImageJ; National Institutes of Health, Bethesda, Maryland, USA).

High resolution confocal imaging of skTM-GFP in live NRVCs was performed on the Leica SP5X confocal system at 37 °C (whole stage incubation chamber; Leica) using a 100X/1.4NA Plan Apo objective lens at a frame rate of 1 h. Epifluorescence imaging was performed on a BZ9000 Fluorescent microscope (Keyence, Osaka, Japan) at 37 °C (stage incubation chamber; Tokai Hit, Shizuoka, Japan) using a 20X/0.75NA objective lens at a frame rate of 1 h. 3D image stacks of 75 x 75 μm (confocal) and 725 x 545 μm (epifluor.) were recorded at 0.75 μm z-section distance throughout the thickness of the sample. Image stacks were maximum-projected prior to kymograph analysis of sarcomere assembly and SCP-growth dynamics (ImageJ; National Institutes of Health, Bethesda, Maryland, USA). Cells were transfected with skTM-GFP using Lipofectamine LTX (Life technologies) according to manufacturer's instructions 36-48 h after siRNA-transfection and 24 h prior to imaging.

Generation of Parvb$^{-/-}$ mice

A *β-parvin* cDNA-containing fragment of EST-clone #2999-a09 (Image: 1193744, GenBank: AA726210) was used to screen a 129/sv mouse P1 artificial chromosome (PAC) library.[82] PAC-clone #597-O14 (Human Genome Mapping Project Center, Cambridge, UK) was used to clone the *Parvb*-targeting construct. A part of exon 2, intron 2 and a part of exon 3 including the putative translation initiation codon 226-228 (M76)[83] were replaced by an internal ribosome entry site (IRES)-regulated lacZ-reporter-gene and a phosphoglycerate-kinase (PGK)-driven neo-resistence cassette, flanked by 5.8kb 5′-end and 2.9kb 3′-end homologous sequences (Figure S1A). After electroporation of the targeting construct into R1 embryonic stem (ES) cells (passage 15), G418-resistent clones were selected as previously described.[84] Briefly, cells were cultured on γ-irradiated embryonic fibroblast cells in DMEM supplemented with 15% FCS, 10^{-4}M β-mercaptoethanol (Sigma-Aldrich) and non-essential amino acids (Thermo Fisher Scientific). After 24 h without selection 300μg/ml G418 (Thermo Fisher Scientific) was added to the medium. After 8-11 days, individual ES-cell colonies were picked into 24 wells and expanded. Half of the 24-well dish was frozen, the other half was used to isolate genomic DNA. Recombinant ES cell clones were identified by radioactive Southern blot of *BamHI*-restricted genomic *DNA* with an *NcoI*/*BamHI*-derived external probe (477 bp of intron 3). Three homologously recombined ES cell clones were used to generate germline chimeric males that produced Parvb$^{+/-}$ mice.

Transverse aortic constriction

Experiments were performed on 2-3 months old control and Parvb$^{-/-}$ mice (including male and female animals) as published.[85] The constriction was generated by tying 6.0 suture twice around a blunt 3 mm segment of a 27 gauge needle, positioned adjacent to the aorta between the right innominate and left carotid arteries. The needle was removed after the constriction was generated. The procedure was performed on anesthetized and ventilated animals according to our approved animal protocol.

Treadmill exercise

Experiments were performed on 3-6-months old control and Parvb$^{-/-}$ mice (including male and female animals). The treadmill (Exer3/6, Columbus Instruments, Columbus, USA) training consisted of a 60 min forced treadmill exercise on five days per week at a velocity of 18 m/min at an angle of 10°. Mice were elicited to run by touching their back with a pencil. Mice were accommodated to the situation for 1 week before starting the experiments. The velocity of 18 m/min was chosen since in pre-experiments control and *β-parvin* knockout mice were able to constantly run for 1 hour at this velocity. An angle of 10° was chosen to increase the muscle load during the training, which was performed for 4 weeks. At the end of this period animals were sacrificed, the hearts were isolated and either fixed in 4% paraformaldehyde (PFA) over 6 h at 4°C for ultrastructural and immunohistochemical analysis, or liquid nitrogen-frozen or immediately treated with RIPA buffer for biochemical analysis. Treadmill exercise and transaortic constriction experiments were performed once.

Please cite this article in press as: Thievessen et al., The focal adhesion protein β-parvin controls cardiomyocyte shape and sarcomere assembly in response to mechanical load, Current Biology (2022), https://doi.org/10.1016/j.cub.2022.05.047

Echocardiography

High-resolution mouse echocardiography was performed using a commercial ultrasound system equipped with a linear array transducer operating at an emission frequency of 15 MHz (harmonic-mode) with frame rates up to 280 Hz (HDI-5000, Philips Medical Systems, Bothell, WA, USA). Axial resolution was 100 μm. Three months old mice were anesthetized with 1.5-1.8% sevoflurane in 50% nitrous oxide/50% oxygen and the constant body temperature was held at 37°C. Data sets were obtained as previously described.[86] Left ventricular end-diastolic and end-systolic volumes, left ventricular mass and ejection fraction (EF) were assessed with the area-length method. Parasternal short-axis views were visually divided into six segments. Imaging was considered adequate when the endocardial and epicardial borders were properly visualized in at least five segments. End-diastolic measurements were obtained at the peak of the R-wave and end-systolic measurements at the time of minimum internal chamber dimensions.

Electron Microscopy

Heart muscle samples were fixed in 4% PFA, rinsed in cacodylate buffer three times and then treated with 1% uranyl acetate in 70% ethanol for 8 h to enhance the contrast. The heart samples were subsequently dehydrated in a graded series of ethanol and then embedded in Araldite (Serva). Semithin sections (0.5 μm) were cut with a glass knife on an ultramicrotome (Reichert, Bensheim, Germany) and stained with methylene blue. Ultrathin sections (30 to 60 nm) for electron microscopic observation were processed on the same microtome with a diamond knife and placed on copper grids. Transmission electron microscopy (TEM) was performed using a 902A electron microscope from Zeiss (Oberkochen, Germany).

Histology and immunohistochemistry

Dissected cardiac and other tissues were fixed in 4% PFA over night (pH 7.2), dehydrated in a graded alcohol series, and embedded in paraffin (Paraplast X-tra; Sigma Aldrich). Sections were cut at 8 μm (HM 355 S, Mikrom, Walldorf, Germany) and stained with hematoxylin/eosin (Thermo Shandon). For immunofluorescence analyses cardiac tissue was frozen in TissueTec-freezing-medium at -80°C. PFA-fixed cryosections (HM 500 OM, Mikrom, Walldorf, Germany) were permeabilized in 0.5% Triton X-100/PBS and blocked in 1% BSA/PBS prior to incubation with primary antibody for 12 h at 4°C at recommended dilutions in 1%BSA/PBS. Secondary antibody incubation was carried out for 1 h at RT. Microscopical analyses were performed on Axioskop (transmitted light) or Axio Imager Z1 (immunofluorescence) microscopes (Zeiss, Germany). For radioactive in situ hybridization, 33P-UTP-labeled (Amersham) sense and antisense riboprobes were generated by *in vitro* transcription (SP6/T7, Invitrogen) from linearized vectors containing α- and β-parvin specific *cDNA* fragments encompassing 500-700 bp long sequences extending from the translated into the 3'-untranslated region of each isoform. Paraffin sections from mouse embryos at different embryonic stages were dewaxed, rehydrated and hybridized as previously described.[87] Microscopical analysis was performed on a MZFLIII binocular (Leica, Bensheim, Germany).

Western and Northern Blots

Liquid nitrogen-frozen or fresh tissue samples were homogenized in 1 ml/0.1 g tissue ice-cold modified RIPA-buffer (50 mM Tris pH 7.4, 150 mM NaCl, 1% Nonidet P40, 0.1% SDS, 0,5% Na-deoxycholate, 1 mM EDTA, 1 mM EGTA, protease-inhibitor cocktail (Roche Complete Mini), phosphatase-inhibitor cocktails (Roche)) per 100 mg tissue with a polytron (30s), dounced 15-20x, incubated on ice for 10 min and centrifuged for 10 min (20000xg, 4°C) to pellet cell debris. 10-20 μg of total protein per lane were SDS gel-separated (reducing conditions), blotted on PVDF membrane and immunoprobed with the primary and secondary antibodies.

For Northern blots 15 μg of Trizol (Invitrogen) extracted total RNA were separated on a 0.8% denaturing agarose gel and transferred to Hybond N+ nylon membranes (Amersham). The membranes were hybridized with 32P-dCTP-labeled (RediPrime II random prime labeling, Amersham) antisense probes (see in situ hybridization) over night at 65°C, expositions (Kodak Biomax MS) for up to 14 days were performed at -80°C.

Rac1 activation assay and GST-PIX pull-down/parvin-GFP co-precipitation

To determine Rac1 activity $2.4x10^6$ freshly isolated NRVCs were plated on collagen I (50 μg/ml Matrix Bioscience #50301) coated culture dishes and transfected with either control or *Parvb*-siRNA after 24 h. 48 h later, cells were lysed in CLB+ buffer (50mM Tris-HCl, 200mM NaCl, 1% NP-40, 10% glycerol, 5mM MgCl2, protease (Roche Complete Mini) and phosphatase (Roche) inhibitors). Biotinylated PAK-CRIB peptide (4-6 μg/40 μl sample) was coupled to Streptavidin-Sepharose beads (Amersham) for 1 h at 4°C and washed 3x (50mM Tris-HCl, 50mM NaCl, 5mM MgCl2, 1mM PMSF and 1 mM DTT). Lysates were incubated with PAK-CRIB peptide coupled beads for 45 min at 4°C and washed 4x with CLB+ buffer, followed by elution of GTP-loaded Rac. Pull down and total lysates samples were subjected to Western blot analysis.

For PIX-parvin co-immunoprecipitation, $1.6x10^6$ COS cells were transfected (Lipofectamine 2000) with the indicated constructs, incubated overnight and lysed in 1ml lysis buffer (150mM TrisHCl pH 8.0, 50mM NaCl, 1mM EDTA, 0,5% NP40, 1 Tablet Roche Complete Mini/10 ml, 0.7 μg/ml pepstatin). 900 μl lysate were incubated for 5 h with glutathione-sepharose beads at 4°C and precipitates were washed with low-salt TBS (50mM TrisHCl pH 7.4, 150mM NaCl) at 6000xg. 20 μl of each total lysate and precipitate were SDS gel-separated under reducing conditions, blotted on PVDF membrane (Roth) and immunoprobed with primary and secondary antibodies.

Please cite this article in press as: Thievessen et al., The focal adhesion protein β-parvin controls cardiomyocyte shape and sarcomere assembly in response to mechanical load, Current Biology (2022), https://doi.org/10.1016/j.cub.2022.05.047

Antibodies

The following antibodies were used: Anti-ILK (#611803; clone 3/ILK, BD Bioscience, WB 1:2000), anti-caveolin-3 (#610421; clone 26/Caveolin 3, BD Bioscience, WB 1:5000), anti-Rac1 (#610651; clone 102/Rac1, BD Bioscience, WB 1:2000), anti-GAPDH (#G8795; clone GAPDH-71.1, Sigma-Aldrich, WB 1:2000), anti-β1 integrin (MAB1997; clone MB1.2, Thermo Fisher Scientific, IF 1:500), anti α-, β- and γ-parvin were described previously[73] (WB 1:1000; IF 1:100), anti-α-actinin (#A7811, Sigma-Aldrich, IHC 1:800), anti-GFP antibody (#8367-2, BD Clontech, WB 1:150), anti-GST-HRP (#GERPN1236, Sigma-Aldrich/GE-Healthcare, WB 1:4000), anti-α-actinin (#ab9465, Abcam, IF 1:500), anti-troponin I (#ab56357, Abcam, IF 1:500), anti-vinculin (#V4505, Sigma-Aldrich, 1:250), anti-PKB/Akt (#9272, Cell Signaling Technology, WB 1:1000), anti-pS473-PKB/Akt (#9271, Cell Signaling Technology, WB 1:1000), TRITC-labeled phalloidin (#P1951, Sigma-Aldrich), anti-mouse-HRP-conjugate (#1706516, BioRad, WB 1:1000), anti-rabbit-HRP-conjugate (#1706515, BioRad, WB 1:1000), fluorescent anti-mouse-, anti-rabbit-, and anti-rat-IgG-conjugates were obtained from Jackson Immunoresearch (#715095151, #715025150, #711225152, #711025152, #712025150, IF 1:500).

QUANTIFICATION AND STATISTICAL ANALYSIS

All image analyses were carried out using Fiji

Statistical analysis

Sample size was not predetermined. Experiments were repeated with independent biological replicates based upon the number of replicates required to obtain consistent results. Unless indicated otherwise, data was reproduced in three independent biological replicates. Individual preparations of primary NRVC or NMVC were scored as biological replicate. All attempts at replication were successful. Data was excluded if positive or negative control samples failed. Mass spec data was filtered for frequently observed contaminants and low confidence uniprot peptides. Mice with pre-conditioned heart abnormalities were excluded. Mice of a specific genotype were randomly allocated to the experimental groups. Investigators were not blinded as the experimental conditions required investigators to know the identity of the samples. Data are presented as mean ± SEM. Statistical analysis and graph production were performed in Graph Prism using one- or two-way ANOVA with post-hoc Bonferroni, or, where indicated, two-tailed Student's t test with unequal variance.